Differential impact of $GABA_A$ Receptors on Inhibitory connectivity for Superficial Pyramidal Neuron Responsiveness *In Vivo*

Yuan-Chen Tsai[1,2], Mohammad Hleihil[1,2], Teresa Cramer[1,2], Kim David Ferrari[1,2], Matthew J.P. Barrett[1,2], Giovanna Bosshard[1], Bruno Weber[1,2], Jillian L. Stobart[1, 3], Shiva K. Tyagarajan[1,2]*

[1]*Institute of Pharmacology and Toxicology, University of Zurich, Winterthurerstrasse 190, 8057 Zurich, Switzerland*

[2]*Center for Neuroscience Zurich (ZNZ), Winterthurerstrasse 190, 8057 Zurich, Switzerland*

[3]*College of Pharmacy, University of Manitoba, Winnipeg, MB R3E 0T5*

*corresponding author
tyagarajan@pharma.uzh.ch

Abstract

A diverse set of $GABA_A$ receptors ($GABA_ARs$) enable synaptic plasticity adaptations at inhibitory postsynaptic sites in collaboration with the scaffolding protein gephyrin. Early studies helped to identify distinctions between $GABA_AR$ subsets allocated within specific functional circuits, but their contribution to the changing dynamics of a microcircuit remains unclear. Here, using the whisker-barrel system we assessed the contribution of specific $GABA_AR$ subtypes to sensory processing *in vivo*. We monitored spontaneous and evoked Ca^{2+} transients in layer 2/3 pyramidal cells with the genetically encoded Ca^{2+} sensor RCaMP1.07. Using *Gabra1* or *Gabra2* global and conditional knockout mice, we uncovered that α1- and α2-$GABA_ARs$ determine the sparseness of L2/3 pyramidal neuron encoding. In a cell-type dependent manner, α1-$GABA_ARs$ affected neuronal excitability while α2-$GABA_ARs$ influenced the reliability of neuronal responses after whisker stimulation. We also discerned that gephyrin and its diverse post-translational modifications (PTMs) facilitate microcircuit homeostasis. Our results underscore the relevance of the diversity of $GABA_ARs$ within a cortical microcircuit.

Introduction

The primary somatosensory cortex (S1) is composed of excitatory and inhibitory neurons that encode passive sensory experience, training on sensory tasks and sensory perceptual learning (Feldman and Brecht 2005). Sensory information is processed in a selective manner and is encoded sparsely. A whisker deflection leads to depolarization in the majority of neurons, but only around 10% of these neurons respond with action potentials (Crochet et al. 2011). In layer 2/3 (L2/3) of the barrel cortex, the excitability of a cortical microcircuit is tightly modulated by inhibitory interneurons (Kapfer et al. 2007). The excitatory neurons outnumber GABAergic interneurons within the neocortex, although precise numbers vary across different cortical areas and layers. In line with this view, the probability of finding excitatory-excitatory connections between 2 pyramidal neurons in supragranular layers is relatively low, whereas the connectivity between pyramidal cells and inhibitory interneurons is much higher (Holmgren et al. 2003; Lefort et al. 2009; Avermann et al. 2012; Petersen 2019). Hence, GABAergic interneurons play a crucial role in controlling the activity of the pyramidal neurons within a cortical microcircuit.

At the postsynaptic sites, $GABA_A$ receptors ($GABA_ARs$) and associated postsynaptic density proteins facilitate downstream signalling to modulate pyramidal cell excitability. In fact, local infusion of the $GABA_AR$ antagonist gabazine leads to increased spontaneous depolarization of L2/3 pyramidal neurons (Gentet et al. 2010). $GABA_ARs$ are assembled from a heterogeneous gene pool to form pentameric ion channels. Apart from differing in their cellular distribution, $GABA_AR$ subtypes also exhibit distinct expression patterns within a given brain circuit (Fritschy and Panzanelli 2014). $GABA_AR$ subtypes are also uniquely localized within different cortical layers. The $\alpha1$ subunit-containing $GABA_ARs$ ($\alpha1$-$GABA_ARs$) are more uniformly distributed across all 6 cortical layers, whereas the $\alpha2$ subunit-containing $GABA_ARs$ are abundantly expressed in the supragranular layers (layer 1, 2 and 3), and the $\alpha3$

subunit containing $GABA_A$Rs are more abundant in layers 5 and 6 (Fritschy and Mohler 1995). This spatial segregation of $GABA_A$R subtype expression likely implies distinct functional roles for $GABA_A$R subtypes within the somatosensory cortex.

$GABA_A$R function is further facilitated by diverse receptor-interacting proteins that include neuroligin-2 (Fritschy, Panzanelli, and Tyagarajan 2012), collybistin (deGroot et al. 2017; Hines et al. 2018) and gephyrin (Tyagarajan and Fritschy 2014). Among these proteins, gephyrin is unique, because it aids activity-dependent GABAergic synapse modulation over different time scales (Battaglia et al. 2018). Many signalling pathways converge onto the gephyrin scaffold and in turn induce diverse post-translational modifications (PTMs) on gephyrin (Zita et al. 2007; Kuhse et al. 2012; Dejanovic and Schwarz 2014; Dejanovic et al. 2014; Ghosh et al. 2016). *In vitro* studies of gephyrin PTMs have offered insights into molecular mechanisms controlling $GABA_A$R availability at postsynaptic sites that may lead to activity-dependent adaptation (Flores et al. 2015; Battaglia et al. 2018). However, the importance and influence of the gephyrin scaffold and its PTMs on microcircuit activity *in vivo* remains unexplored.

Analysis of circuit connectivity and interneuron cooperativity within the barrel cortex has helped to delineate the importance of GABAergic inhibition in coordinating pyramidal neuron activity (Petersen 2014). At the microcircuit level, parvalbumin-expressing (PV+) neurons that typically synapse onto pyramidal cell soma and proximal dendrites become activated during passive and active whisker sensing. In contrast, somatotatin-expressing (SOM+) interneurons that typically synapse onto distal dendrites of a pyramidal cell become hyperpolarized during whisker sensing (Gentet et al. 2012). The importance of inhibition is even more prominent in awake mice as cortical state changes from quiet to active whisker behaviour involves the reorganization of GABAergic neuronal network activity (Gentet et al. 2010). Pyramidal neuron response to different interneuron function during sensory processing

relies heavily on the downstream receptor complex and postsynaptic density proteins. Hence, within a cortical microcircuit, differential $GABA_AR$ activation within principal cell must encode sensory inputs. Currently, the identities of specific $GABA_ARs$ and the role of scaffolding proteins in determining cortical microcircuit functional specificity is unknown.

In this study, we examined the involvement of specific $GABA_AR$ subtypes, namely α1-$GABA_AR$ and α2-$GABA_AR$, and gephyrin for sensory input-dependent cortical microcircuit function. In this regard, we employed a genetically encoded Ca^{2+} sensor, RCaMP1.07, to measure Ca^{2+} transients in L2/3 pyramidal neurons in the barrel cortex in wild type (WT) and *Gabra1* or *Gabra2* global and conditional gene deficient mice. We report different functional roles for α1- and α2-$GABA_AR$ subtypes, and the main scaffolding protein gephyrin for neuronal population activity upon whisker stimulation. We identify that at a global level, α1-$GABA_ARs$ determine excitability of L2/3 pyramidal neurons and α2-$GABA_ARs$ determine response reliability of pyramidal neurons to sensory stimulation. However, within pyramidal cells, both α1- and α2-$GABA_ARs$ control sparseness within the responding population. Gephyrin scaffold dynamics help fine tune L2/3 pyramidal neuron excitability by contributing to $GABA_AR$ subtype recruitment to inhibitory postsynaptic sites. Taken together, the changing needs of the barrel cortex L2/3 microcircuit is facilitated by specific $GABA_AR$ subtypes and their recruitment via the dynamic gephyrin scaffold.

Results

$GABA_AR$ subtypes adapt their expression to altered sensory inputs

To determine whether GABAergic synapses are involved in activity-dependent plasticity in the barrel cortex, we assessed whether $GABA_AR$ cell surface expression was altered in response to sensory stimulation or sensory deprivation. We injected an AAV8 virus encoding tdTomato under the control of the CaMKIIα promoter into the lateral ventricles on

post-natal day 0 (P0) to achieve wide-scale tdTomato expression in excitatory neurons, including cortical pyramidal cells (Kim et al. 2013). At P60, we either stimulated the vibrissae bilaterally for 1 minute every day or trimmed all the whiskers daily for 1 week (Fig. 1A). The mice were then sacrificed and tdTomato-positive L2/3 pyramidal neurons in the barrel cortex were analysed for expression of $GABA_AR$ subtypes using immunohistochemistry for GABRA1 or GABRA2 proteins, as α1- or α2-$GABA_AR$ represent the most abundant $GABA_ARs$ in the cortex (Fritschy and Mohler 1995) (Fig. 1B, C). Cluster analysis with an Image-J plugin (see methods for details) was performed to identify GABRA1 or GABRA2 puncta at the somata, where synapses are mostly inhibitory, and the α1- or α2-$GABA_AR$ cluster density and size were determined (Fig. 1D-G). The α1-$GABA_AR$ cluster density was reduced after 1-week of whisker stimulation or whisker trimming ($F_{(2, 11)}$=37.18, P<0.0001; Fig. 1D). In contrast, α1-$GABA_AR$ cluster size was increased after 1-week whisker stimulation but did not change after whisker trimming ($F_{(2,10)}$=4.6, P=0.036; Fig. 1E). In contrast, α2-$GABA_AR$ cluster density was not changed after either stimulation or trimming ($F_{(2,10)}$=2.27, P=0.153; Fig. 1F), but their cluster size increased in the whisker stimulation group ($F_{(2,10)}$=6.45, P=0.016; Fig. 1G). Together, altered sensory inputs to the barrel cortex led to dramatic reduction in number of somatic α1-$GABA_AR$ clusters, and the size of α1- and α2-$GABA_AR$ clusters increased slightly upon whisker stimulation for a week. These results indicate that $GABA_AR$ subtypes adapt differently to changes in sensory input, suggesting that these receptor subtypes may have different functions in sensory processing.

α1-$GABA_A$Rs contribute to sparse pyramidal neuron activity during sensory encoding

To evaluate the functional role of α1-$GABA_ARs$ in sensory processing, we made use of the *Gabra1* gene deletion mouse line (Vicini et al. 2001). We employed longitudinal *in vivo* 2-photon Ca^{2+} imaging of L2/3 pyramidal neurons populations in the barrel cortex of *Gabra1*

knockout mice (under 1.2% isoflurane). AAV6-CaMKIIα-RCaMP1.07, a red-shifted genetically encoded Ca^{2+} indicator (Ohkura et al. 2012) driven by the CaMKIIα promoter, was used to measure activity change specifically within pyramidal L2/3 neurons (Fig. 2A). After 4 weeks of viral transgene expression, spontaneous and single whisker stimulation-induced Ca^{2+} transients were imaged. In the trials with whisker stimulation, we used a 1-second 90 Hz single-whisker stimulation protocol with a piezo-based stimulator (Mayrhofer et al. 2015; Stobart et al. 2018), and it started 2.5 seconds after the trial initiation. In order to capture the stimulus-induced Ca^{2+} transients, our analysis was restricted to the time during and after 1 second of whisker stimulation (Figure 2a; right panel). Changes in neuronal activity were assessed by analysing Ca^{2+} transients for parameters such as amplitude, duration at half-maximum of amplitude, and number of events per imaging session (40 trials).

Analysis for spontaneous Ca^{2+} transients in the same time window demonstrated no change between WT and *Gabra1* KO mice (Fig. 2B; Suppl. Fig. 1B-B''). However, in *Gabra1* KO animals L2/3 pyramidal neurons exhibited a higher amplitude of Ca^{2+} transients after whisker stimulation (Fig. 2C). Analysis for duration and the number of events per neuron (over 40 trials) did not show differences in average values between WT and *Gabra1* KO (Fig. 2C'-C''). Also, the time of onset and decay time of Ca^{2+} events were similar in WT and *Gabra1* KO (Suppl. Fig. 1C-C').

Pyramidal neuron activity *in vivo* indicates that roughly 10% of the population in L2/3 barrel cortex encodes sensory stimulation with robust, high amplitude Ca^{2+} events due to sparse firing (Crochet et al. 2011), even though the Ca^{2+} response magnitude is broadly distributed across the population (Fig. 2C). Based on this knowledge, and to understand how *Gabra1* gene depletion impacts the population distribution of pyramidal neuron activity, we defined a cut-off for high-responding cells as the 90th percentile amplitude value from the WT neurons and only considered L2/3 pyramidal neurons in the WT and KO groups that had amplitudes greater

than or equal to this value (Margolis et al. 2012). In WT mice, these high responders were 11% of the total population, while high responders with amplitudes over the same cut-off mark were 36% of the *Gabra1* KO principal cells (Fig. 2D). This likely accounted for the higher signal amplitudes observed in the *Gabra1* KO population (Fig. 2C). When we compared the Ca^{2+} transient amplitude, duration and number of events within this subset of high-responding neurons, we did not find any difference between the 2 genotypes, apart from a reduction in the duration of spontaneous Ca^{2+} transients in *Gabra1* KO mice (Fig. 2E-E''). Our results show that α1-$GABA_A$Rs contribute to controlling pyramidal neuron excitability after whisker stimulation and sparseness within the population.

α2-$GABA_A$Rs regulate reliability of L2/3 pyramidal cell responding to sensory inputs

Next, we evaluated the role of α2-$GABA_A$Rs using a *Gabra2* gene deletion mouse line (*Gabra2* KO) (Panzanelli et al. 2011; Koester et al. 2013). Similar to the results described above, spontaneous or stimulation-induced pyramidal neuron Ca^{2+} transients were measured (Fig. 3A-A'). Analysis of spontaneous Ca^{2+} transients showed no genotype effect on amplitude (Suppl. Fig. 2B). Upon whisker stimulation, we observed a bimodal distribution of signal amplitudes in *Gabra2* KO. The majority of cells had lower than average amplitude signals and a small sub-group had higher than average amplitude responses than in WT, although the mean amplitudes between WT and *Gabra2* KO were not different (Fig. 3B). The duration of spontaneous Ca^{2+} transients were similar between WT and *Gabra2* KO (Suppl. Fig. 2B'); however, after whisker stimulation, Ca^{2+} transients tended to have a shorter duration ($p=0.13$; Fig. 3B'). When considering the number of Ca^{2+} events per neuron across all trials, the frequency of spontaneous activity was similar between *Gabra2* KO and WT cells (Suppl. Fig. 2B''), but whisker stimulation evoked fewer (~50%) Ca^{2+} transients in *Gabra2* KO, indicating a reduced reliability of pyramidal neurons to repetitively encode whisker stimulation (Fig.

3B''). In addition, we observed slower onset and longer decay time of Ca^{2+} transients after whisker stimulation in *Gabra2* KO compared to WT (Suppl. Fig. 2C-C').

To evaluate whether *Gabra2* gene deletion also influences the population distribution of highly responsive pyramidal neurons, we set a cut-off according to the amplitudes of the WT group as described in the previous section. Using this amplitude value, we found 21% of pyramidal neurons were high responders in *Gabra2* KO mice (Fig. 3C). Within this subset, the amplitude of both spontaneous and whisker stimulation-induced Ca^{2+} transients in *Gabra2* KO was higher than in WT high-responders (Fig. 3D), while there was no difference in the duration of spontaneous or whisker stimulation-induced events (Fig. 3D'). Although the number of events per neuron occurring under spontaneous activity was not different between high amplitude pyramidal neurons of each genotype, the number of events evoked by whisker stimulation was reduced in *Gabra2* KO (Fig. 3D''). Our data suggests that α2-$GABA_A$Rs influence the success rate of whisker stimulation-triggered neuronal responses, and partially contribute to the sparseness of the high-responding pyramidal neurons by increasing the neuronal activity in a small set of the neuronal population.

Potential compensation from other widely expressed α subunits in *Gabra1* or *Gabra2* KO could influence our *in vivo* findings. Using Western blot analysis from barrel cortex tissue, we measured expression changes in α2 and α3 subunits of *Gabra1* KO and α1 and α3 subunits of *Gabra2* KO (Suppl. Fig. 3). As shown previously (Kralic et al. 2006), expression of the α3 subunit was increased in *Gabra1* KO with no change in α2 subunit levels (Suppl. Fig. 3A, A'). In *Gabra2* KO tissue, we also found an increase in α3 subunit expression but no change in α1 subunit expression (Suppl. Fig. 3B, B'). Although α3 subunit expression levels are increased in both α1 and α2 KOs, this increased expression of α3 is unlikely to account for observed effects on Ca^{2+} transients, since the effects of Ca^{2+} transients are different between the α1 and α2 KOs.

Cell autonomous effects of GABA$_A$R subtypes within barrel cortex microcircuits

To further specify the contribution of α1- and α2-GABA$_A$Rs to the output of L2/3 microcircuits, we specifically ablated the *Gabra1* or *Gabra2* gene from adult pyramidal neurons using either *Gabra1$^{flox/flox}$* or *Gabra2$^{flox/flox}$* mice. We injected AAV6-CaMKIIα-RCaMP1.07 (Area 1) or co-injected AAV6-CaMKIIα-eGFP-Cre and AAV6-CaMKIIα-RCaMP1.07 (Area 2) into neighbouring barrel cortex areas and compared Ca^{2+} transients from Cre-positive and Cre-negative cells between barrels or within the same barrel (Suppl. Fig. 4A-D). As a control, we compared spontaneous transients in RCaMP1.07-only expressing cells within Area 1 and Area 2 to confirm that the baseline activity of the RCaMP-only cells from Area 2 were not altered compared with Area 1 cells (Suppl. Fig. 4E).

Next, we quantified changes in RCaMP1.07 transients in *Gabra1$^{flox/flox}$* mice. Similar to *Gabra1* KO, the pyramidal cell-specific Cre expression did not increase the amplitude and the number of events for spontaneous Ca^{2+} transients after α1-GABA$_A$R deletion compared with Cre-negative cells in the same barrel (Suppl. Fig. 4F). There was a modest increase in duration of spontaneous Ca^{2+} transients after Cre expression (Suppl. Fig. 4F'). After whisker stimulation, we observed a reduction in the amplitude and number of Ca^{2+} transients in Cre-expressing L2/3 pyramidal neurons (Fig. 4A, 4A"). There was no change in the duration of Ca^{2+} transients (Fig. 4A'). We examined how the frequency of high responders changed after L2/3 pyramidal neuron-specific α1-GABA$_A$R deletion. Upon whisker stimulation, we established a cut-off for 12% of high amplitude responders in RCaMP-only expressing cells and using the same cut-off criteria, we found that in *Gabra1$^{flox/flox}$* Cre-expressing cells there were no high responders (Fig. 4B). This absence of highly responsive cells upon α1-GABA$_A$R deletion in pyramidal neurons is consistent with the reduction in amplitude observed after whisker stimulation. Together, our data identified that in the absence of α1-GABA$_A$Rs, L2/3 pyramidal neurons exhibit reduced excitability and impairment in the recruitment of high

responding neurons during whisker stimulation. Our result implies that $GABA_AR$ within interneuron subtypes differentially affect the activity of pyramidal neurons. Additionally, α1-$GABA_ARs$ regulate the number of responding cells and the magnitude of Ca^{2+} response as a population.

We next assessed for Ca^{2+} transient changes between Cre-positive or RCaMP1.07-only positive cells in *Gabra2*$^{flox/flox}$ mice. Similar to the global *Gabra2* KO, we observed no significant differences in spontaneous Ca^{2+} transients in *Gabra2*$^{flox/flox}$ Cre expressing cells (Suppl. Fig. 4G-G''). Upon whisker stimulation, there was no change in the mean peak amplitude, duration and number of events in Cre-positive cells (Fig. 4C-C''). When determining the proportion of high responding pyramidal neurons after whisker stimulation using a 90th percentile amplitude cut-off value in RCaMP-only expressing neurons, there was an increased number of high responders (18%) in *Gabra2*$^{flox/flox}$ Cre-expressing cells (Fig. 4D). In these *Gabra2*$^{flox/flox}$ mice, high responders demonstrated no difference in amplitude and duration under both spontaneous and whisker stimulation-induced conditions (Fig. 4E-E''). Unlike *Gabra2* KO neurons that exhibited a reduction in number of events (Fig. 3D-D''), the Cre-expressing high responders demonstrated an increased number of events ($p=0.007$). This suggested that α2-$GABA_ARs$ in different neuronal subtypes within L2/3 barrel cortex contribute both directly and indirectly to pyramidal neuron excitability upon whisker stimulation. In *Gabra2*$^{flox/flox}$ (Fig. 4D), L2/3 pyramidal neurons exhibited increased representation of the whisker stimulus, which demonstrates that both α1- and α2-$GABA_ARs$ in pyramidal neurons regulate the number of responding cells, albeit in opposite directions. Therefore, the two $GABA_AR$ subtypes are functionally distinct within pyramidal neurons.

Gephyrin scaffold dynamics influence GABAergic neurotransmission in vivo

Synaptic $GABA_ARs$ are associated with the scaffolding protein gephyrin, which enables downstream signalling at inhibitory postsynaptic sites and allows for dynamic adaptation to changes in excitatory transmission (Tyagarajan and Fritschy 2014). The gephyrin scaffold has been shown to interact with several effector proteins at inhibitory postsynaptic sites. The dynamic adaptations of gephyrin scaffolding have been reported to be regulated by diverse post-translational modifications (PTMs), up- or down-regulating GABAergic neurotransmission (Ghosh et al. 2016). α1- or α2-$GABA_ARs$ are known gephyrin interactors, with distinct properties (Tretter et al. 2012); hence, we aimed to understand the importance of gephyrin scaffold reorganization at these synapses and its functional impact on an intact circuit. To study the role of activity-dependent gephyrin adaptations, we selected 3 distinct gephyrin mutant variants that have been reported to impact its scaffolding properties: a SUMO1 conjugation-defective mutant (K148R) that has been reported to rescue sub-membrane gephyrin clustering in *Gabra2* KO neurons (Ghosh et al. 2016); phosphorylation-null mutants S303A/S305A (SSA), where phosphorylation of these residues by protein kinase A (PKA) and calcium calmodulin kinase II α (CaMKIIα) is required for NMDA receptor-dependent $GABA_AR$ recruitment at the synapse (Flores et al. 2015); and a dominant-negative (DN) mutant lacking the last 12 amino acids that has been reported to disrupt gephyrin scaffolding and GABAergic neurotransmission *in vitro* (Ghosh et al. 2016) (Fig. 5A).

To assess the functional impact of these 3 gephyrin mutants on GABAergic neurotransmission in L2/3 pyramidal neurons, we injected AAV6-hSyn1-flex-eGFP-gephyrin variants, AAV6-CaMKIIα-ERT2-Cre and AAV6-CaMKIIα-RCaMP1.07 to co-express eGFP-gephyrin variants and RCaMP1.07 in L2/3 principal cells (Fig. 5B). This combination of viruses was also used to evaluate activity changes in pyramidal neurons with *in vivo* 2-photon Ca^{2+} imaging (see next section). After 4 weeks of virus co-expression, we injected tamoxifen intraperitoneally (i.p) to induce Cre expression. First, we recorded miniature inhibitory

postsynaptic currents (mIPSC) from L2/3 pyramidal neurons overexpressing the respective gephyrin transgenes in acute slices of barrel cortex in the presence of tetrodotoxin (TTX), CNQX and AP-5 (Fig. 5C). Neurons expressing the transgene gephyrin-DN demonstrated reduced mIPSC amplitude (14.6 ± 1.6 pA) with respect to GFP controls (28.8 ± 2.0 pA; P<0.0001). The mIPSC frequency was also decreased in gephyrin-DN neurons (inter event intervals: 1451 ± 463.2 ms; GFP=659.9 ± 78.3 ms; P=0.038; Fig. 5D). It is known that gephyrin-DN destabilizes synaptic $GABA_A$Rs *in vitro*, and perhaps a similar mechanism reduces synaptic $GABA_A$R availability in gephyrin-DN-expressing neurons. Next, neurons expressing the transgene with gephyrin-SSA mutation demonstrated mIPSCs of increased amplitude (37.8 ± 2.7 pA; P=0.026; Fig. 5D), likely as a result of increased $GABA_A$R retention at synaptic sites (Battaglia et al. 2018). Finally, the expression of gephyrin transgene with the K148R mutation had no effect on mIPSC amplitude compared to controls (28.8 ± 2.0 pA vs 25.6 ± 1.8 pA; P=0.641). Apart from gephyrin-DN, the inter-event interval (IEI) was not different between the gephyrin mutants (eGFP: 659.9 ± 78.3 ms; gephyrin-K148R: 408.0 ± 56.3 ms; gephyrin-SSA: 401 ± 73.7 ms), suggesting that there were no major changes in spontaneous neurotransmitter release or in the number of GABAergic inhibitory synapses (Fig. 5D). Overall, our results show that the majority of the GABAergic postsynaptic sites containing gephyrin are influenced by cellular signaling events that directly impact PTMs on gephyrin. Importantly, different gephyrin mutants influence GABAergic neurotransmission in a mutually exclusive manner. Hence, gephyrin mutants are novel tools to manipulate pyramidal neuron excitability during whisker stimulation.

Gephyrin mutant expression influences whisker stimulation-induced Ca^{2+} transients

Next, we measured changes in Ca^{2+} transients in pyramidal neurons before and after gephyrin-mutant expression. Gephyrin-mutant expression was controlled by tamoxifen

inducible Cre expression. We confirmed that around 40% of the pyramidal cells co-expressed all 3 viral vectors (Suppl. Fig. 5). As an additional control, we expressed RCaMP1.07 in a neighbouring barrel area (Area 1) (Fig. 6A). We examined all RCaMP-expressing neurons and compared changes in Ca^{2+} transients before and after eGFP-gephyrin expression. Examples of average Ca^{2+} transient changes in response to whisker stimulation both before and after gephyrin-mutant expression are shown (Fig. 6B). The activity of individual neurons was normalized to activity before tamoxifen injection [(After-Before)/Before] to identify relative changes.

Gephyrin-mutant expression did not influence spontaneous Ca^{2+} transient amplitude and number of events compared to the control (area1) (Suppl. Fig. 6A, A''). However, gephyrin-K148R mutant expression reduced spontaneous event duration (Suppl. Fig. 6A'). Upon whisker stimulation, gephyrin-mutant expression effects on Ca^{2+} transients were consistent with the patch clamp recording results (Fig. 5). The gephyrin-K148R mutant caused no change in any of the parameters (Fig. 5C-C"). The gephyrin-SSA mutant expression decreased the amplitude of evoked events, while the gephyrin-DN mutant tended to increase the amplitude of Ca^{2+} transients but the overall effect was not significant compared to the control (P=0.373; Fig. 6C). The duration of Ca^{2+} transients was mostly unaffected by expression of gephyrin mutants (Fig. 6C'). Expression of the gephyrin-SSA and gephyrin-DN mutants reduced and increased the number of events, respectively (Fig. 6C''). Furthermore, onset and decay times were similar before and after expression of gephyrin variants (Fig. 6D). We previously identified high responders in conditional and total α1- and α2-$GABA_AR$ KO (Figs. 2-4) to determine the influence of these receptor subtypes on L2/3 pyramidal neuron excitability and high responder recruitment during sensory inputs. We used a similar strategy to group neurons based on their Ca^{2+} transients amplitude or number of events within our gephyrin mutant populations. As expected, in control neurons from Area 1, the amplitude and

number of events within the populations remained comparable before and after tamoxifen injection (Suppl. Fig. 6B). Similarly, gephyrin-K148R mutant expression did not impact the population distribution based on amplitude changes. However, expression of gephyrin-SSA and gephyrin-DN mutants had the most impact on amplitude changes within the given population of neurons. Specifically, gephyrin-SSA mutant expression led to a smaller population of neurons responding with high amplitude, while on the other hand gephyrin-DN mutant expression increased the population of high amplitude neurons by 20%. The number of Ca^{2+} transient event distributions was not affected upon gephyrin-K148R or gephyrin-SSA expression but was vastly increased in gephyrin-DN mutant expressing L2/3 pyramidal neurons. Specifically, the cell population exhibiting 21-30 events increased from 29% to 49% and 31-40 events increased from 4% to 10%. Overall, our data identifies the gephyrin scaffold as an essential component for response reliability to sensory inputs, and modulations of the gephyrin scaffold in a subset of pyramidal neurons were sufficient to fine-tune the population response to whisker stimulation.

Discussion:

Somatosensory information is processed in a selective manner and is encoded sparsely. While it is well established that GABAergic inhibition plays a central role in sparse sensory processing, the contribution of $GABA_AR$ subtypes to the functional specificity of the somatosensory cortex microcircuit is unknown. To fill this knowledge gap, our current study employed different combinations of gene manipulations to modify specific components of GABAergic postsynapse and examine changes in L2/3 barrel cortex microcircuit excitability *in vivo*. We report that neuronal expression of α1- and α2-$GABA_ARs$ were differentially altered after sensory stimulation and deprivation. Within the L2/3 microcircuit, α1- and α2-$GABA_ARs$ influenced distinct aspects of sparse sensory processing. The α1-$GABA_ARs$

impacted the amplitude of Ca^{2+} transients, while α2-$GABA_A$Rs contributed to the reliability of neuronal responses to whisker stimulation. The opposite observations between global α1-$GABA_A$R- and α2-$GABA_A$R gene deletion animal models, and between conditional pyramidal neuron specific α1- and α2-$GABA_A$R KOs suggests differential functional contributions for $GABA_A$R subtypes within interneurons and principal neurons. Furthermore, we uncovered that gephyrin fine tunes neuronal excitability within a functional circuit. Our results provide evidence for the regulatory role of gephyrin PTMs in L2/3 pyramidal neuron responses upon sensory inputs.

Neuronal network activity defined by $GABA_A$R subtypes

Barrel cortex plasticity is a multifaceted process involving multiple synaptic and cellular mechanisms. While recruitment of silent neurons into the active neuronal population is an important plasticity mechanism, the role of $GABA_A$R subtypes in defining this network connectivity change remains poorly characterized. Our data posits that $GABA_A$R subtypes are well placed to regulate various aspects of synaptic plasticity mechanisms to recruit silent neurons into the active population. However, whether any specificity exists between a $GABA_A$R subtype and a subgroup of interneuron is highly debatable. It has been proposed that specific $GABA_A$R subtypes are allocated to distinct interneuron terminals, thereby defining a functional circuit. For example, it has been suggested that α1-$GABA_A$Rs are localized at PV+ basket cell terminals, while α2-$GABA_A$Rs are localized at CCK+ cell terminals (Nyíri, Freund, and Somogyi 2001; Freund 2003). However, it was subsequently reported that α1 and α2-$GABA_A$R subtypes can be localized at both CCK+ and PV+ terminals (Kerti-Szigeti and Nusser 2016). While the α-subunit has been long thought to be an essential factor determining the allocation of $GABA_A$Rs to different postsynaptic sites, it was recently reported that $GABA_A$Rs containing β3 subunits are allocated specifically to PV+ terminals but not SOM+

connections (Nguyen and Nicoll 2018). Hence, there are multiple molecular determinants underlying $GABA_AR$ synapse allocation and these factors add an additional layer of complexity to understanding circuit activity.

In hippocampal pyramidal neurons, α2-$GABA_ARs$ are preferentially expressed at the axon-initial segment (AIS) when compared with α1- or α3-containing $GABA_ARs$ (Nusser et al. 1996; Muir and Kittler 2014). In the somatosensory cortex, this compartmentalized distribution of $GABA_AR$ subunits is less clear, as α1, α2 and α3 subunits exhibit a similar distribution ratio between the AIS compartment and non-AIS compartment (Gao and Heldt 2016). Subcellular localization differences between $GABA_ARs$ is also influenced by lateral surface mobility in response to network activity changes, thereby contributing to synaptic scaling mechanisms (Bannai et al. 2009). Specifically, at AIS, α2-$GABA_ARs$ show lower mobility compared to α1-$GABA_ARs$ (Muir and Kittler 2014), therefore, the abundance of α2-$GABA_ARs$ at synapses might facilitate membrane depolarization to a greater extent than other $GABA_AR$ subtypes. It has been reported that stimulating GABAergic axo-axonic cells can elicit action potentials in the postsynaptic pyramidal neurons from L2/3 somatosensory cortex (Szabadics et al. 2006). Hence, α1- and α2-$GABA_ARs$ at AIS are well positioned to facilitate pyramidal neuron excitability.

$GABA_AR$ subtypes facilitate sparse encoding in L2/3 pyramidal cells

Sparse coding within pyramidal neurons is determined by changes in excitation-inhibition balance (Andermann and Moore 2006). The L2/3 pyramidal neurons have more hyperpolarized resting potentials; therefore, they require more excitatory input and/or reduced GABAergic input to overcome the action potential threshold (Lefort et al. 2009). Our data demonstrates that $GABA_AR$ subtypes within L2/3 pyramidal neurons are well placed to contribute to circuit-specific sub-threshold excitation and sparse action potential firing. Using

Gabra1 and *Gabra2* KO mice, we demonstrate that a greater proportion of pyramidal neurons become high-responders upon whisker stimulation. In our experiments, specificity of cortical responses towards the corresponding whisker remained unaltered in the absence of α1- or α2-$GABA_A$Rs, as we were able to visualize barrel activity by both intrinsic optical imaging of blood flow and *in vivo* 2-photon Ca^{2+} imaging. These observations imply that distinct $GABA_A$R subtypes promote sensory input-dependent activity change in L2/3 pyramidal neurons. This enhancement is an indirect effect of α1- or α2-$GABA_A$R function in interneurons or subcortical regions that affect the L2/3 microcircuit. Perhaps, the α5-$GABA_A$Rs are also well placed to contribute to activity-dependent plasticity as it has been reported that extrasynaptic α5-$GABA_A$Rs receptors can be recruited to synaptic sites (Renner et al. 2012).

We also elucidated that the α2-$GABA_A$Rs determine the reliability of pyramidal neuron excitability within L2/3 barrel cortex. Based on our results, we suspect that α2-$GABA_A$Rs contribute to disrupted interconnectivity between L2/3 pyramidal neurons but increased fidelity within interneurons of the microcircuit. This idea is supported by independent observations demonstrating that removal of α2-$GABA_A$R in pyramidal neurons leads to more pyramidal neurons being recruited as high responders, while global *Gabra2* gene deletion reduces the number of events in pyramidal neurons (Fig. 3B''). Hence, the reduction in number of events is likely to be an indirect effect of enhancing recurrent inhibition from the microcircuit. Taken together, our data provide evidence for distinct $GABA_A$R subtype function in L2/3 connectivity.

In our experiments, we obtained up to 40% co-expression of eGFP-gephyrin mutants with RCaMP and Cre within the L2/3 pyramidal neurons. In spite of this small-scale co-infectivity ratio, we successfully perturbed microcircuit function upon gephyrin-mutant expression in the barrel cortex. Importantly, we identified an important role for cellular signalling and gephyrin scaffold PTMs in fine-tuning GABAergic inhibition. Disruption of the

gephyrin scaffold through the expression of the gephyrin-DN-mutant led to an expansion in neuronal populations with higher amplitude in Ca^{2+} transients. On the other hand, expression of the gephyrin-SSA mutant led to a decrease in the number of high responder cells (suppl. Fig. 6). Our gephyrin mutants allowed us to specifically manipulate GABAergic postsynaptic sites, as evident from changes in mIPSC amplitude and IEI (Fig. 5D). Although a population of gephyrin-independent $GABA_A$Rs are present, the gephyrin-containing inhibitory synapses functionally dominate and facilitate dynamic shifts in Ca^{2+} transient amplitude adjustments within high responding neurons (Suppl. Fig. 6B).

Gephyrin scaffold dynamics drive homeostatic adaptations within L2/3 microcircuit

It is currently hypothesized that both Hebbian and non-Hebbian synaptic plasticity mechanisms might underlie strengthening and weakening of cellular responses after whisker stimulation and/or trimming (Turrigiano and Nelson 2000; Hofer et al. 2011; Crochet et al. 2011; Margolis et al. 2012). Our data identified a role for homeostatic plasticity mechanisms within cortical L2/3 microcircuits during sensory encoding. In *Gabra1* and *Gabra2* KO mice, the average amplitude increased and number of events of Ca^{2+} transients decreased respectively, while the ratio of high responders increased in both KO models (Fig. 4). On the other hand, results from *Gabra1*$^{flox/flox}$ and *Gabra2*$^{flox/flox}$ mice demonstrated a reduction in average amplitude and no change in the number of events of Ca^{2+} transients, respectively. These observed functional adaptations in opposite directions suggest that homeostatic mechanism(s) at the level of the microcircuit are influenced by $GABA_A$R subtypes within both pyramidal neurons and interneurons.

The gephyrin scaffold is known to interact with α1-$GABA_A$Rs and α2-$GABA_A$Rs (Tyagarajan and Fritschy 2014). Independent quantum dot–based single-$GABA_A$R tracking studies have shown that the gephyrin scaffold influences $GABA_A$R surface mobility and

synapse retention (Choquet and Triller 2013). Specifically, it was recently shown that gephyrin PTMs, specifically the gephyrin-SSA mutant increases the synaptic confinement of α2-$GABA_A$Rs in response to 4-Aminopyridine-induced circuit activation (Battaglia et al. 2018). Our electrophysiology data demonstrated an increase in mIPSC amplitude in gephyrin-SSA expressing neurons (Fig. 5). *In vivo* imaging data showed that a less excitable population of neurons doubled in size upon gephyrin-SSA expression and whisker stimulation (Suppl. Fig. 6B). Increased synaptic confinement of α2-$GABA_A$Rs in gephyrin-SSA expressing neurons could disrupt dynamic shifts in synaptic inhibition to maintain microcircuit homeostasis. We have demonstrated that gephyrin-DN expression increased diffusion and exploration of α2-$GABA_A$Rs at both synaptic and extrasynaptic sites (Battaglia et al. 2018). In our electrophysiology studies, we observed increases in mIPSC IEI and reduced amplitude upon gephyrin-DN mutant expression (Fig. 5). *In vivo* imaging data demonstrated that gephyrin-DN mutant expression increases the population of high responders after whisker stimulation by 20% (Suppl. Fig. 6B). Our data implicate a dynamic recruitment model for specific $GABA_AR$ subtypes based on gephyrin PTM. This would mean that specific demand would trigger a signalling cascade to converge onto the gephyrin scaffold. The PTM change on gephyrin in turn would switch affinity towards specific $GABA_AR$ subtype for synapse recruitment. Independent of gephyrin scaffold modulation, a mechanism involving microRNA miR376c was recently reported to specifically regulate dendritic α1 and α2 subunit expression after inhibitory long-term potentiation (iLTP), but not α3, α4, α5 subunit containing $GABA_A$Rs (Rajgor et al. 2020). This highlights a role for multiple context-dependent $GABA_AR$ modulation at inhibitory synapses.

In summary, while it is known that the distribution of activity within cortical neurons is sparse, our data demonstrates that pyramidal neuron excitability is defined by $GABA_A$ receptor subtypes and facilitated by gephyrin scaffold dynamics. Our results have characterized

for the first-time molecular components that are operational at GABAergic postsynaptic terminals to refine and define the sparse sensory encoding process in adult mice.

Methods

All experiments were performed in accordance with the European Community Council Directives of November 24, 1986 (86/609/EEC) and approved by the cantonal veterinary office of Zurich.

Animals

Male and female mice C57BL/6J were purchased (Charles River, Germany), and the following strains were maintained in house: FVB, *Gabra1* KO (Vicini et al., 2001), *Gabra2* KO (Panzanelli et al., 2011; Koester et al., 2013), *Gabra1*$^{flox/flox}$ (Vicini et al., 2001), *Gabra2*$^{flox/flox}$ (Duveau et al., 2011). Control groups were sex-matched with the experimental groups. They were group-housed in an inverted 12-hour light/dark cycle. All mice underwent surgery at 8-12 weeks of age and were imaged repeatedly (2-4 times per week) under a 2-photon microscope for up to 5 months.

Cloning and virus production

The AAV2/6-CaMKIIa-RCaMP1.07 construct was generated by cloning of the RCaMP1.07 gene (Ohkura et al., 2012; Pilz et al., 2015) into an adeno-associated plasmid backbone (AAV2) under a calcium/calmodulin dependent protein kinase II alpha (CaMKIIα) promoter.

The eGFP-gephyrin-K148R, eGFP-gephyrin-DN, eGFP-gephyrin S303/305A expression vectors have been described previously (Flores *et al*., 2015; Ghosh *et al*., 2016), and were subcloned into an AAV2 plasmid backbone containing the human synapsin1 (hSyn1) promoter, in an inverted orientation, and flanked by 2 different loxP sites. The transgene was

packaged into AAV 6 serotype. All the AAV6 recombinant viruses were generated by the Viral Vector Core at the University of Zürich. AAV2/6-CaMKIIa-CreERT2 virus was purchased from Vector Biolabs (#2014-1208).

Lateral ventricle viral injection

C57BL/6 mouse pups received bilateral viral injection into lateral ventricle at post-natal day 0 (P0) (Kim et al. 2013). In short, P0 pups were briefly anaesthetized with isoflurane, and 2 μl viral solution per lateral ventricle was injected using a 10 μl Hamilton syringe with a 32 gauge. Lateral ventricles were targeted using bregma and lambda as reference points to draw the mid-line, the needle was inserted into a site 1 mm lateral from the mid-point of the mid-line perpendicular to the skin surface. The needle was inserted to a depth of 3 mm into the skull to ensure injection into the lateral ventricle. Virus used for the experiments was AAV8-CaMKIIa-tdTomato in the control and experimental groups. The injected pups were placed back in their home cage after waking up from anesthesia. The mice were housed under normal conditions until 2-months of age when they were then used for experiments.

Tamoxifen administration

Tamoxifen (1 mg per animal; Sigma, T5648) was given intraperitoneally (i.p.) for 4 consecutive days to induce Cre recombinase activity from CreERT2. The neurons expressing the transgene were imaged 5-7 days post final tamoxifen injection.

Surgery and virus injections for 2-photon Ca^{2+} imaging

Surgical procedures were divided into 2 steps, which were 2-4 days apart. In the first surgery, after fixing the mouse head in a stable position in a stereotaxic frame, an incision was made along the mid line to expose the skull. After cleaning the bone, bonding reagent (ONE

COAT 7 Universal, Coltene) was applied, and then a head cap was created using layers of light-cured dental cement (SYNERGEY D6 Flow, Coltene). Finally, the custom-made aluminium head post was attached to the head cap. These procedures were carried out under isoflurane (4% for induction and 1.5-2% for maintenance, Forene, AbbVie). The second surgery involved a craniotomy, cortical viral injection and chronic window implantation. With a dental drill, a small piece of skull was removed above the sensory cortex to expose the barrel cortex. A glass pipette and hydraulic pump were used to inject 150 nL of virus (injecting speed 50-70 nL per minute) at a depth of 350 μm beneath the brain surface into the whisker areas identified by Intrinsic optical imaging (see below). Immediately after the injections, a 3x3 mm coverslip was fixed right above the exposed brain and secured with dental cement to the head cap. Buprenorphine (Temgesic 0.1 mg/kg) was given before and after surgical procedures for 3 days.

Intrinsic optical imaging (IOI)

IOI was used to identify barrel areas of the corresponding whiskers in the left somatosensory cortex. This technique was used to image activation of barrel areas through the skull (before craniotomy) to map the whisker field for potential viral injections, and through the cranial window to map specific whisker areas before 2-photon imaging. Under a red light (630 nm illumination), the activated brain region (imaged 400 μm under cortical surface) was identified by increased light absorption following whisker deflection by a piezo stimulator. Imaging was done by using a 12-bit CCD camera (Pixelfly VGA, PCO imaging), and the animals were maintained under 1-1.2% isoflurane.

Two-photon imaging

A custom-built 2-photon laser-scanning microscope (Mayrhofer et al. 2015) with a 20x water immersion objective (W Plan-Apochromat 20x/1.0 DIC VIS-IR, Zeiss) was used for *in vivo* Ca^{2+} imaging in anaesthetized mice. The microscope was equipped with a Ti:sapphire laser (Mai Tai; Spectra-Physics) set to 1040 nm to excite RCaMP1.07. Fluorescence emission was detected with GaAsP photo-multiplier modules (Hamamatsu Photonics) fitted with a 520/50 nm band pass filter or a 607/70 band pass filter and separated by 560 nm dichroic mirror (BrightLine; Semrock). A customized version of ScanImage (r3.8.1; Janelia Research Campus) was used for setting imaging parameters and to control the microscope.

Confirmation of viral expression at the injected site and neuronal activation during whisker stimulation was examined first, before the series of imaging sessions. Every imaging session comprised 40 trials of spontaneous activity and 40 trials with whisker deflection (90 Hz, 1 s, piezo-based stimulator), while the duration of each trial was 15 s. Fast images were taken (11.84 Hz, 128x128 pixels) to capture neuronal Ca^{2+} responses. Imaging depth ranged from 160-200 μm beneath the cortical surface, which was in layer 2/3 of the barrel cortex. Once a field of view was selected, the same field was imaged for 3-4 sessions on different days, and an extra 3 sessions if the animals were subjected to tamoxifen injections.

Western Blot analysis

Barrel cortices from both hemispheres were isolated surgically and lysed mechanically in EBC lysis buffer (50 mM Tris-HCl, 120 mM NaCl, 0.5% NP-40, and 5 mM EDTA) containing a protease inhibitor cocktail (cOmplete™, Mini Protease Inhibitor Cocktail, Roche) and phosphatase inhibitors (Phosphatase Inhibitor Cocktail 2, Phosphatase Inhibitor Cocktail 3, Sigma-Aldrich), and then incubated for 1 hour on ice. The lysates were then centrifuged at 23,000 rpm (~48,500 rcf) for 30 minutes. Samples were prepared for loading by mixing 30 μg of protein in 5xSDS sample buffer containing 15% 2-Mercaptoethanol (Bio-Rad) and heated

at 90 °C for 5 minutes. Then samples were loaded onto 8% SDS-polyacrylamide gels and run in Tris-glycine buffer at room temperature. Gels were transferred to a PVDF membrane. The membranes were blocked for 1 hour at room temperature with 5% blocking agent (Roche Diagnostic) in TBST (100 rpm shaker). Primary antibodies in blocking solution were then added to the membrane and incubated overnight at 4 °C (100 rpm shaker). After washing with TBST, the membranes were then incubated for 1 hour at room temperature with secondary antibodies coupled to either horseradish peroxidase or IRDye® (LI-COR) to visualize the protein bands with either film (FujiFilm) or Odyssey imager (LI-COR). Intensity of the bands were quantified using ImageJ. The levels of GABRA1, GABRA2 and GABRA3 were normalized to actin levels.

Immunohistochemistry

All mice were perfused with ice cold artificial cerebrospinal fluid (ACSF; 125 mM NaCl, 2.5 mM KCl, 1.25 mM NaH_2PO_4, 26 mM $NaHCO_3$, 25 mM D-glucose, 2.5 mM $CaCl_2$, and 2 mM $MgCl_2$), which was oxygenated (95% O_2, 5% CO_2) for 30 minutes. After isolating the brains, the tissues were subjected to 90 minutes post fixation in 4% paraformaldehyde (PFA) at 4˚C. The post-fixed brain was left overnight in 30% sucrose at 4˚C for cryo-protection. The frozen brains were cut into 40 μm thick coronal sections by using microtome and stored in anti-freeze buffer. Sections within the coverage of the barrel field were selected and stained for the α1 or α2 $GABA_AR$ subunit (see antibody list) and an appropriate secondary antibody was used to visualize the receptor localization. The images (1024x1024 pixels) were captured using a confocal LSM 700 microscope (Zeiss) and synaptic clusters were analysed using ImageJ image-processing plugin (github repository: https://github.com/dcolam/Cluster-Analysis-Plugin). Z-stack images were taken to cover the cell body and its apical dendrite, and these images were then collapsed into 2D images for cluster analysis. Auto-thresholding

moments method was applied. A mask over the somatic region was created for every analysed neuron (10-15 neurons per mouse, 4-5 mice per group) and the mask was enlarged by a factor of 1. Colocalization analysis was then performed for GABRA1 or GABRA2 staining. GABRA1 or GABRA2 particles were identified if the sizes fell within the range between 0.03 μm and 5 μm. Imaging and image processing were performed under blinded condition.

Electrophysiology

Mice were sacrificed by cervical dislocation. The brains were removed quickly and immersed in ice-cold cutting solution (110 mM sucrose, 60 mM NaCl, 3 mM KCl, 1.25 mM NaH_2PO_4, 28 mM $NaHCO_3$, 0.5 mM $CaCl_2$, 7 mM $MgCl_2$, 5 mM D-glucose). 300 μm coronal slices of the virus-injected area of the somatosensory cortex were made using a Leica VT1200 vibratome (Leica Biosystems). The slices were incubated at 32˚C for 30 minutes in ACSF (125 mM NaCl, 2.5 mM KCl, 1.25 mM NaH_2PO4, 26 mM $NaHCO_3$, 25 mM D-glucose, 2.5 mM $CaCl_2$, and 2 mM $MgCl_2$). After the recovery period, slices were maintained at RT with continuous perfusion of carbogenated ACSF (95% O_2, 5% CO_2). All recordings were performed at RT. Sampling rate was 10kHz.

Recordings were amplified by Multiclamp 700B amplifier and digitized with Digidata 1440 (Molecular Devices). The recording electrode was pulled from a borosilicate glass pipette (3–5 MΩ) using an electrode puller (PC-100, NARISHIGE Group). For recordings of miniature inhibitory post synaptic currents (mIPSCs), pipettes were filled with caesium-based solution containing 120 mM CsCl, 10 mM EGTA, 10 mM HEPES pH 7.4, 4 mM $MgCl_2$, 0.5 mM GTP and 2 mM ATP. Events were isolated by adding CNQX (25 μM, Merck), AP-5 (50 μM, almone labs) and tetrodotoxin (1 μM, Affix Scientific). 10 min after establishing the whole-cell mode, mIPSCs were analysed for a duration of 2 min. Events were recorded using Clampex 10.7 software (Molecular Devices). Recordings were filtered offline using a Bessel

low pass filter at 500 Hz (Clampfit 10.7, Molecular Devices) and analysed using MiniAnalysis 6.0.7 software (Synaptosoft).

Two-Photon quantification and statistical analysis

All individual neurons expressing RCaMP1.07 in a field of view were manually selected as regions of interest (ROIs) on ImageJ and further processed with custom-designed toolbox Cellular and Hemodynamic Image Processing Suite (CHIPS; Barrett et al., 2018) for MATLAB (R2015b, MathWorks). The images for a field of view were first motion-corrected with a 2D convolution engine for x-y drift. The dF/F value from each manually selected ROI was calculated relative to the baseline imaging period before whisker stimulation (the 2.5 seconds from the beginning of each trial). Peaks were identified by the MATLAB findpeaks function following application of a digital band-pass filter (passband frequency of minimum 0.1 Hz and maximum 2 Hz) and a threshold of 5 standard deviations from the baseline. The peak onset time was calculated by the first time point of the smoothed signal trace (2 frames moving average) crossed over the threshold (the mean of the 2.5 seconds baseline plus 1.5 times the standard deviation) after the start of stimulation.

For the analysis, we focused on the 2 second time window indicated in Fig. 2A (1 second of whisker stimulation and 1 second after the stimulation). For the high responders, the cut-off points for amplitude and number of events were defined as ~10% of the neuronal population in WT of the corresponding experiment. The size of the population, amplitude, duration and number of events of the high responders were analysed separately.

Statistical analysis was performed using R (version 3.5.3) with the multcomp package for linear-mixed effect model. We set the following as fixed effects which were tested individually or for their interactions: stimulation condition (with or without whisker stimulation), genotype (for *Gabra1* KO and *Gabra2* KO experiments), Cre (for *Gabra1*$^{flox/flox}$

and *Gabra2*$^{flox/flox}$ experiment, with or without Cre expression), treatment with TAM (for the gephyrin mutant experiment, before or after tamoxifen injections), mutants (for gephyrin the mutant experiment, to compare between different mutants). Individual animal and ROIs were set as random effects. The data were presented with means (un-corrected) and standard error of the means (SEM). The p values reported for different comparisons were obtained by using a Tukey post-hoc test.

Acknowledgements

We thank J-M. Fritschy for comments on the manuscript and M. Müller for comments on the electrophysiology data. The study was supported by UZH Forschungskredit Can-doc grant to Y-C. Tsai, Olga Mayenfisch Foundation grant, Swiss National Science Foundation grant (310030_192522) and University of Zurich internal funding to S.K. Tyagarajan.

Author contributions

SKT and YCT conceptualised the study. SKT, YCT, BW and JLS contributed to the design of experiments. YCT performed all 2-photon imaging experiments, data analysis and wrote the first draft of the manuscript. All authors contributed to the writing and editing of the manuscript. SKT, BW, JLS, KDF and MJPB provided technical knowledge and data analysis support. MH carried out electrophysiological experiments and the analysis. TC helped with the morphological staining and analysis.

Competing financial interests

The authors declare no competing financial interests.

References

Andermann, Mark L, and Christopher I Moore. 2006. “A Somatotopic Map of Vibrissa Motion Direction within a Barrel Column.” *Nature Neuroscience* 9 (4): 543–51. https://doi.org/10.1038/nn1671.

Avermann, Michael, Christian Tomm, Celine Mateo, Wulfram Gerstner, and Carl C. H. Petersen. 2012. “Microcircuits of Excitatory and Inhibitory Neurons in Layer 2/3 of Mouse Barrel Cortex.” *Journal of Neurophysiology* 107 (11): 3116–34. https://doi.org/10.1152/jn.00917.2011.

Bannai, Hiroko, Sabine Lévi, Claude Schweizer, Takafumi Inoue, Thomas Launey, Victor Racine, Jean-Baptiste Sibarita, Katsuhiko Mikoshiba, and Antoine Triller. 2009. “Activity-Dependent Tuning of Inhibitory Neurotransmission Based on GABAAR Diffusion Dynamics.” *Neuron* 62 (5): 670–82. https://doi.org/10.1016/j.neuron.2009.04.023.

Battaglia, Sereina, Marianne Renner, Marion Russeau, Etienne Côme, Shiva K. Tyagarajan, and Sabine Lévi. 2018. “Activity-Dependent Inhibitory Synapse Scaling Is Determined by Gephyrin Phosphorylation and Subsequent Regulation of GABAA Receptor Diffusion.” *ENeuro* 5 (1): ENEURO.0203-17.2017. https://doi.org/10.1523/ENEURO.0203-17.2017.

Choquet, Daniel, and Antoine Triller. 2013. “The Dynamic Synapse.” *Neuron* 80 (3): 691–703. https://doi.org/10.1016/J.NEURON.2013.10.013.

Crochet, Sylvain, James F.A. Poulet, Yves Kremer, and Carl C.H. Petersen. 2011. “Synaptic Mechanisms Underlying Sparse Coding of Active Touch.” *Neuron* 69 (6): 1160–75. https://doi.org/10.1016/j.neuron.2011.02.022.

Dejanovic, Borislav, and Guenter Schwarz. 2014. “Brief Communications Neuronal Nitric Oxide Synthase-Dependent S-Nitrosylation of Gephyrin Regulates Gephyrin Clustering at GABAergic Synapses.” https://doi.org/10.1523/JNEUROSCI.0531-14.2014.

Dejanovic, Borislav, Marcus Semtner, Silvia Ebert, Tobias Lamkemeyer, Franziska Neuser, Bernhard Lüscher, Jochen C. Meier, and Guenter Schwarz. 2014. "Palmitoylation of Gephyrin Controls Receptor Clustering and Plasticity of GABAergic Synapses." Edited by Matthew B.Dalva. *PLoS Biology* 12 (7): e1001908. https://doi.org/10.1371/journal.pbio.1001908.

Feldman, Daniel E., and Michael Brecht. 2005. "Map Plasticity in Somatosensory Cortex." *Science*. MIT Press. https://doi.org/10.1126/science.1115807.

Flores, Carmen E., Irina Nikonenko, Pablo Mendez, Jean-Marc Fritschy, Shiva K. Tyagarajan, and Dominique Muller. 2015. "Activity-Dependent Inhibitory Synapse Remodeling through Gephyrin Phosphorylation." *Proceedings of the National Academy of Sciences* 112 (1): E65–72. https://doi.org/10.1073/pnas.1411170112.

Freund, Tamás F. 2003. "Interneuron Diversity Series: Rhythm and Mood in Perisomatic Inhibition." *Trends in Neurosciences* 26 (9): 489–95. https://doi.org/10.1016/S0166-2236(03)00227-3.

Fritschy, Jean-Marc, and Hanns Mohler. 1995. "GABAA-receptor Heterogeneity in the Adult Rat Brain: Differential Regional and Cellular Distribution of Seven Major Subunits." *Journal of Comparative Neurology* 359 (1): 154–94. https://doi.org/10.1002/cne.903590111.

Fritschy, Jean-Marc, and Patrizia Panzanelli. 2014. "GABAA Receptors and Plasticity of Inhibitory Neurotransmission in the Central Nervous System." *European Journal of Neuroscience* 39 (11): 1845–65. https://doi.org/10.1111/ejn.12534.

Fritschy, Jean-Marc, Patrizia Panzanelli, and Shiva K. Tyagarajan. 2012. "Molecular and Functional Heterogeneity of GABAergic Synapses." *Cellular and Molecular Life Sciences* 69 (15): 2485–99. https://doi.org/10.1007/s00018-012-0926-4.

Gao, Yudong, and Scott A. Heldt. 2016. "Enrichment of GABAA Receptor α-Subunits on the

Axonal Initial Segment Shows Regional Differences." *Frontiers in Cellular Neuroscience* 10 (March): 39. https://doi.org/10.3389/fncel.2016.00039.

Gentet, Luc J., Michael Avermann, Ferenc Matyas, Jochen F. Staiger, and Carl C.H. Petersen. 2010. "Membrane Potential Dynamics of GABAergic Neurons in the Barrel Cortex of Behaving Mice." *Neuron* 65 (3): 422–35. https://doi.org/10.1016/J.NEURON.2010.01.006.

Gentet, Luc J, Yves Kremer, Hiroki Taniguchi, Z Josh Huang, Jochen F Staiger, and Carl C H Petersen. 2012. "Unique Functional Properties of Somatostatin-Expressing GABAergic Neurons in Mouse Barrel Cortex." *Nature Neuroscience* 15 (4): 607–12. https://doi.org/10.1038/nn.3051.

Ghosh, Himanish, Luca Auguadri, Sereina Battaglia, Zahra Simone Thirouin, Khaled Zemoura, Simon Messner, Mario A. Acuña, et al. 2016. "Several Posttranslational Modifications Act in Concert to Regulate Gephyrin Scaffolding and GABAergic Transmission." *Nature Communications* 7: 1–16. https://doi.org/10.1038/ncomms13365.

deGroot, Claire, Amalia Floriou-Servou, Yuan-ChenTsai, Simon Früh, Manuela Kohler, Georgia Parkin, Cornelia Schwerdel, et al. 2017. "RhoGEF9 Splice Isoforms Influence Neuronal Maturation and Synapse Formation Downstream of A2 GABAAreceptors." *PLoS Genetics* 13 (10): 1–27. https://doi.org/10.1371/journal.pgen.1007073.

Hines, Rochelle M., Hans Michael Maric, Dustin J. Hines, Amit Modgil, Patrizia Panzanelli, Yasuko Nakamura, Anna J. Nathanson, et al. 2018. "Developmental Seizures and Mortality Result from Reducing GABAA Receptor A2-Subunit Interaction with Collybistin." *Nature Communications* 9 (1): 1–15. https://doi.org/10.1038/s41467-018-05481-1.

Hofer, Sonja B., Ho Ko, Bruno Pichler, Joshua Vogelstein, Hana Ros, Hongkui Zeng, Ed Lein, Nicholas A. Lesica, and Thomas D. Mrsic-Flogel. 2011. "Differential

Connectivity and Response Dynamics of Excitatory and Inhibitory Neurons in Visual Cortex." *Nature Neuroscience* 14 (8): 1045–52. https://doi.org/10.1038/nn.2876.

Holmgren, Carl, Tibor Harkany, Björn Svennenfors, and Yuri Zilberter. 2003. "Pyramidal Cell Communication within Local Networks in Layer 2/3 of Rat Neocortex." *Journal of Physiology* 551 (1): 139–53. https://doi.org/10.1113/jphysiol.2003.044784.

Kapfer, Christoph, Lindsey L Glickfeld, Bassam V Atallah, and Massimo Scanziani. 2007. "Supralinear Increase of Recurrent Inhibition during Sparse Activity in the Somatosensory Cortex." *Nature Neuroscience* 10 (6): 743–53. https://doi.org/10.1038/nn1909.

Kerti-Szigeti, Katalin, and Zoltan Nusser. 2016. "Similar GABAA Receptor Subunit Composition in Somatic and Axon Initial Segment Synapses of Hippocampal Pyramidal Cells." *ELife* 5 (AUGUST). https://doi.org/10.7554/eLife.18426.001.

Kim, Ji Yoen, Ryan T. Ash, Carolina Ceballos-Diaz, Yona Levites, Todd E. Golde, Stelios M. Smirnakis, and Joanna L. Jankowsky. 2013. "Viral Transduction of the Neonatal Brain Delivers Controllable Genetic Mosaicism for Visualising and Manipulating Neuronal Circuits in Vivo." *European Journal of Neuroscience* 37 (8): 1203–20. https://doi.org/10.1111/ejn.12126.

Koester, Christina, Uwe Rudolph, Tatjana Haenggi, Aurélie Papilloud, Jean-Marc Fritschy, and Florence Crestani. 2013. "Dissecting the Role of Diazepam-Sensitive γ-Aminobutyric Acid Type A Receptors in Defensive Behavioral Reactivity to Mild Threat." *Pharmacology Biochemistry and Behavior* 103 (3): 541–49. https://doi.org/10.1016/J.PBB.2012.10.004.

Kralic, Jason E., Corinne Sidler, Franziska Pakpan, Gregg E. Homanics, A. Leslie Morrow, and Jean-Marc Fritschy. 2006. "Compensatory Alteration of Inhibitory Synaptic Circuits in Cerebellum and Thalamus of γ-Aminobutyric Acid Type A Receptor A1 Subunit

Knockout Mice." *Journal of Comparative Neurology* 495 (4): 408–21. https://doi.org/10.1002/cne.20866.

Kuhse, Jochen, Heba Kalbouneh, Andrea Schlicksupp, Susanne Mükusch, Ralph Nawrotzki, and Joachim Kirsch. 2012. "Phosphorylation of Gephyrin in Hippocampal Neurons by Cyclin-Dependent Kinase CDK5 at Ser-270 Is Dependent on Collybistin." *The Journal of Biological Chemistry* 287 (37): 30952–66. https://doi.org/10.1074/jbc.M112.349597.

Lefort, Sandrine, Christian Tomm, J.-C. Floyd Sarria, and Carl C.H. Petersen. 2009. "The Excitatory Neuronal Network of the C2 Barrel Column in Mouse Primary Somatosensory Cortex." *Neuron* 61 (2): 301–16. https://doi.org/10.1016/j.neuron.2008.12.020.

Margolis, David J., Henry Lütcke, Kristina Schulz, Florent Haiss, Bruno Weber, Sebastian Kügler, Mazahir T. Hasan, and Fritjof Helmchen. 2012. "Reorganization of Cortical Population Activity Imaged throughout Long-Term Sensory Deprivation." *Nature Neuroscience* 15 (11): 1539–46. https://doi.org/10.1038/nn.3240.

Mayrhofer, Johannes M., Florent Haiss, Fritjof Helmchen, and BrunoWeber. 2015. "Sparse, Reliable, and Long-Term Stable Representation of Periodic Whisker Deflections in the Mouse Barrel Cortex." *NeuroImage* 115 (July): 52–63. https://doi.org/10.1016/J.NEUROIMAGE.2015.04.045.

Moretto Zita, M., Ivan Marchionni, Elisa Bottos, Massimo Righi, Giannino Del Sal, Enrico Cherubini, and Paola Zacchi. 2007. "Post-Phosphorylation Prolyl Isomerisation of Gephyrin Represents a Mechanism to Modulate Glycine Receptors Function." *EMBO Journal* 26 (7): 1761–71. https://doi.org/10.1038/sj.emboj.7601625.

Muir, James, and Josef T. Kittler. 2014. "Plasticity of GABAA Receptor Diffusion Dynamics at the Axon Initial Segment." *Frontiers in Cellular Neuroscience* 8 (June): 151. https://doi.org/10.3389/fncel.2014.00151.

Nguyen, Quynh Anh, and Roger A. Nicoll. 2018. “The GABAA Receptor β Subunit Is Required for Inhibitory Transmission.” *Neuron* 98 (4): 718-725.e3. https://doi.org/10.1016/j.neuron.2018.03.046.

Nusser, Z, W Sieghart, D Benke, J-M Fritschy, and P Somogyi. 1996. “Differential Synaptic Localization of Two Major Gamma-Aminobutyric Acid Type A Receptor Alpha Subunits on Hippocampal Pyramidal Cells.” *Proceedings of the National Academy of Sciences of the United States of America* 93 (21): 11939–44. https://doi.org/10.1073/pnas.93.21.11939.

Nyíri, Gábor, Tamás F. Freund, and PéterSomogyi. 2001. “Input-Dependent Synaptic Targeting of A2-Subunit-Containing GABAA Receptors in Synapses of Hippocampal Pyramidal Cells of the Rat.” *European Journal of Neuroscience* 13 (3): 428–42. https://doi.org/10.1046/j.1460-9568.2001.01407.x.

Ohkura, Masamichi, Takuya Sasaki, Chiaki Kobayashi, Yuji Ikegaya, and Junichi Nakai. 2012. “An Improved Genetically Encoded Red Fluorescent Ca2+ Indicator for Detecting Optically Evoked Action Potentials.” *PLoS ONE* 7 (7). https://doi.org/10.1371/journal.pone.0039933.

Panzanelli, Patrizia, Benjamin G. Gunn, Monika C. Schlatter, Dietmar Benke, Shiva K. Tyagarajan, Peter Scheiffele, Delia Belelli, Jeremy J. Lambert, Uwe Rudolph, and Jean-Marc Fritschy. 2011. “Distinct Mechanisms Regulate GABA A Receptor and Gephyrin Clustering at Perisomatic and Axo-Axonic Synapses on CA1 Pyramidal Cells.” *Journal of Physiology* 589 (20): 4959–80. https://doi.org/10.1113/jphysiol.2011.216028.

Petersen, Carl C. H. 2019. “Sensorimotor Processing in the Rodent Barrel Cortex.” *Nature Reviews Neuroscience*, July, 1–14. https://doi.org/10.1038/s41583-019-0200-y.

Petersen, Carl C.H. 2014. “Cell-Type Specific Function of GABAergic Neurons in Layers 2 and 3 of Mouse Barrel Cortex.” *Current Opinion in Neurobiology*.

https://doi.org/10.1016/j.conb.2013.10.004.

Rajgor, Dipen, Alicia M. Purkey, Jennifer L. Sanderson, Theresa M. Welle, Joshua D. Garcia, Mark L. Dell'Acqua, and Katharine R. Smith. 2020. "Local MiRNA-Dependent Translational Control of GABAAR Synthesis during Inhibitory Long-Term Potentiation." *Cell Reports* 31 (12): 107785. https://doi.org/10.1016/j.celrep.2020.107785.

Renner, Marianne, Claude Schweizer, Hiroko Bannai, Antoine Triller, and Sabine Lévi. 2012. "Diffusion Barriers Constrain Receptors at Synapses." Edited by FabienTell. *PLoS ONE* 7 (8): e43032. https://doi.org/10.1371/journal.pone.0043032.

Stobart, Jillian L., Kim David Ferrari, Matthew J.P. Barrett, Chaim Glück, Michael J. Stobart, Marc Zuend, and Bruno Weber. 2018. "Cortical Circuit Activity Evokes Rapid Astrocyte Calcium Signals on a Similar Timescale to Neurons." *Neuron* 98 (4): 726-735.e4. https://doi.org/10.1016/j.neuron.2018.03.050.

Szabadics, János, Csaba Varga, Gábor Molnár, Szabolcs Oláh, Pál Barzó, and Gábor Tamás. 2006. "Excitatory Effect of GABAergic Axo-Axonic Cells in Cortical Microcircuits." *Science* 311 (5758): 233–35. https://doi.org/10.1126/science.1121325.

Tretter, Verena, Jayanta Mukherjee, Hans Michael Maric, Hermann Schindelin, Werner Sieghart, and Stephen J. Moss. 2012. "Gephyrin, the Enigmatic Organizer at GABAergic Synapses." *Frontiers in Cellular Neuroscience*. Frontiers. https://doi.org/10.3389/fncel.2012.00023.

Turrigiano, Gina G., and Sacha B. Nelson. 2000. "Hebb and Homeostasis in Neuronal Plasticity." *Current Opinion in Neurobiology*. Current Biology Ltd. https://doi.org/10.1016/S0959-4388(00)00091-X.

Tyagarajan, Shiva K., and Jean-Marc Fritschy. 2014. "Gephyrin: A Master Regulator of Neuronal Function?" *Nature Reviews Neuroscience* 15 (3): 141–56.

https://doi.org/10.1038/nrn3670.

Vicini, S, C Ferguson, K Prybylowski, J Kralic, A L Morrow, and G E Homanics. 2001. "GABA(A) Receptor Alpha1 Subunit Deletion Prevents Developmental Changes of Inhibitory Synaptic Currents in Cerebellar Neurons." *The Journal of Neuroscience : The Official Journal of the Society for Neuroscience* 21 (9): 3009–16. https://doi.org/10.1523/JNEUROSCI.21-09-03009.2001.

Figure Legends

Figure 1. $GABA_AR$ subunit expression changes after altered sensory input. (A) An overview of bilateral viral injections into lateral ventricles at P0, followed by stimulation (Stim) or whisker trimming (Trim) protocol for 1 week prior to morphology analysis on individual pyramidal neurons. Trim group, the whiskers were trimmed bilaterally every day to the same length as the facial hair. The Stim group received daily 1 minute of large angle whisker deflection bilaterally. (B) Representative images of L2/3 pyramidal neurons in barrel cortex from control, trim and stim groups expressing α1-$GABA_AR$ subunit. (C) Representative images of L2/3 pyramidal neurons in barrel cortex from control, trim and stim groups expressing α2-$GABA_AR$ subunit. (D-E) Quantification of cluster analysis of density and size for α1-$GABA_AR$ from N=4 mice for control and trim groups, N=5 for Stim group. (F-G) Quantification of cluster analysis of density and size for α2-$GABA_AR$. In total, 10-15 neurons were imaged per mouse and data points represent average of individual animals. Statistics: One-way ANOVA, with Bonferroni post hoc test. Error bar: standard deviation. *$p \leq 0.05$, **$p \leq 0.01$, ***$p \leq 0.001$.

Figure 2. L2/3 pyramidal neuron activity changes in Gabra1 KO mice. (A) Overview of virus injection protocol for *in vivo* 2-photon imaging. AAV6-CaMKIIa-RCaMP virus was

injected to the barrel cortex. After 1-month, the mice were subjected to a series of imaging composed of spontaneous and whisker stimulation imaging sessions, and each session composed of forty 15-second trials (with 3-second inter-trial interval). Each whisker stimulation trial consisted 1 second of 90 Hz whisker stimulation after 2.5 seconds of baseline. **(B)** Average trace example of spontaneous and whisker stimulation imaging sessions. Grey bar: whisker stimulation. Standard deviations are shown in lighter colors under the example trace. **(C-C'')** Average Ca^{2+} transient amplitude, duration and number of events in whisker stimulation trials in density plots and bar graphs (insets). The average was obtained from all imaging sessions for individual neurons (N=459 neurons from 5 *Gabra1* KO mice, N=418 neurons from 4 WT mice). **(D)** Proportions of high and lower responding cells selected based on ~10% of high Ca^{2+} transient amplitude versus rest. (E- E'') Quantification of amplitude, duration or number of events between the high responders of WT and *Gabra1* KO. Statistics: linear mixed-effects models and Tukey post hoc tests. All bar graphs are represented as mean ± SEM. *$p \leq 0.05$, **$p \leq 0.01$, ***$p \leq 0.001$.

Figure 3. L2/3 pyramidal neuron activity change in *Gabra2* KO mice. (A) Average trace from an example of spontaneous and whisker stimulation imaging session. Grey bar: whisker stimulation. Standard deviations are shown in lighter colors below the example trace. **(B-B')** Average Ca^{2+} transient amplitude, duration and number of events in whisker stimulation trials in density plots and bar graphs (insets). N=370 neurons from 4 *Gabra2* KO mice, N=307 neurons from 3 WT mice. **(C)** Proportions of high and lower responding cells selected based on ~10% of high Ca^{2+} transient amplitude versus rest. **(D-D'')** Quantification of amplitude, duration and the number of events measured both high responders in WT and *Gabra2* KO. Statistics: linear mixed-effects models and Tukey post hoc tests. All bar graphs are represented as mean ± SEM. *$p \leq 0.05$, **$p \leq 0.01$, ***$p \leq 0.001$.

Figure 4. L2/3 pyramidal neuron activity change in *Gabra1*$^{flox/flox}$ and *Gabra2*$^{flox/flox}$ mice. (A-A'') Stimulation-induced Ca^{2+} transient amplitude, duration and number of events in whisker stimulation trials in density plots and bar graphs (insets) comparing RCaMP-expressing neurons and RCaMP/CaMKIIα-eGFP-Cre neurons from *Gabra1*$^{flox/flox}$ mice. N=34 RCaMP-expressing neurons and N=47 RCaMP/CaMKIIα-eGFP-Cre expressing neurons from area2 of *Gabra1*$^{flox/flox}$ mice. **(B)** Proportions of high- and lower-responding cells selected based on 90th percentiles of stimulation-induced Ca^{2+} transient amplitude change in RCaMP-expressing and RCaMP/CaMKIIα-eGFP-Cre expressing neurons from *Gabra1*$^{flox/flox}$ mice. **(C-C'')** Stimulation-induced Ca^{2+} transient amplitude, duration and number of events in whisker stimulation trials in density plots and bar graphs (insets) comparing RCaMP-expressing neurons and RCaMP/CaMKIIα-eGFP-Cre expressing neurons from *Gabra2*$^{flox/flox}$ mice. N=58 RCaMP-expressing neurons and N=132 RCaMP/CaMKIIα-eGFP-Cre neurons from *Gabra2*$^{flox/flox}$ mice. **(D)** Proportions of high- and lower-responding cells selected based on top 90th percentiles of stimulation-induced Ca^{2+} transient amplitude changes in RCaMP-expressing and RCaMP/CaMKIIα-eGFP-Cre expressing neurons from *Gabra2*$^{flox/flox}$ mice. **(E-E'')** Averaged amplitude, duration and the number of events between the high responders in RCaMP-expressing and RCaMP/CaMKIIα-eGFP-Cre expressing neurons from *Gabra2*$^{flox/flox}$ mice. Statistics: linear mixed-effects models and Tukey post hoc tests. All bar graphs are represented as mean ± SEM. *$p \leq 0.05$, **$p \leq 0.01$, ***$p \leq 0.001$.

Figure 5. GABAergic neurotransmission changes in gephyrin-mutant-expressing L2/3 pyramidal neurons. (A) An illustration of different gephyrin mutations used in the study, along with the signalling pathways that are known to impact the mutated residues are shown. The gephyrin-K148R (SUMO1 conjugation site mutant) facilitates scaffolding. The gephyrin-

S303A and gephyrin-S305A (PKA and CaMKIIα phospho-null mutant) hampers NMDAR activity-induced scaling at GABAergic postsynaptic sites. The gephyrin-DN (lacks part of E domain) disrupts endogenous gephyrin scaffolds in neurons. **(B)** Representative images of neuron co-labelling after AAV virus infection *in vivo*. The following combination of viruses were injected to the barrel cortex (same combination used in 2P Ca^{2+} imaging): AAV6-hSyn1-flex-gephyrin mutant, AAV6-CaMKIIa-CreERT2, AAV6-CaMKIIa-RCaMP1.07. All brain sections were stained for CaMKIIα and eGFP. **(C)** Example traces from L2/3 pyramidal cells expressing gephyrin mutants or GFP control. Colored traces: averaged current from one neuron. Grey traces: all events measured from one neuron. **(D)** Miniature inhibitory postsynaptic currents (mIPSCs) amplitude and inter-event interval (IEI) in L2/3 pyramidal neurons expressing individual gephyrin mutant. Statistics: eGFP, n=23; K148R, n=13; gephyrin-DN, n=13; gephyrin-SSA, n=10 neurons, from 4-5 mice. One-way ANOVA with Tukey post-hoc test. Bars: mean ± SEM. *$p \leq 0.05$, **$p \leq 0.01$, ***$p \leq 0.001$, ****$p \leq 0.0001$.

Figure 6. Gephyrin mutant expression influences L2/3 pyramidal neuron excitability changes. (A) An overview of the viral infection *in vivo*. The control site (Area 1) received only AAV6-CaMKIIα-RCaMP1.07, while the experimental site (Area 2) received a combination of RCaMP/CaMKIIα-eGFP-Cre/gephyrin viruses. **(B)** Average trace examples from imaging sessions for whisker stimulation trials of both before and after gephyrin mutant expression. Grey bar: whisker stimulation. Lighter colors around the example trace are standard deviations. **(C-C'')** Average percentage changes after gephyrin-mutant expression for individual neurons are shown in bar graphs and the ratios are shown as violin plots to demonstrate the distribution differences in stimulation-induced Ca^{2+} transients. **(D)** Onset and decay time for before and after expression of the gephyrin mutants. eGFP, n=491 neurons; gephyrin-K148R, n=308 neurons; gephyrin-SSA, n=249 neurons; gephyrin-DN, n=204 neurons. Statistics: linear

mixed-effects models and Tukey post hoc tests. All bar graphs are represented as mean ± SEM. *p≤0.05, **p≤0.01, ***p≤0.001.

Suppl. Figure 1. Spontaneous L2/3 pyramidal neuron activity in Gabra1 KO mice. (A) Field of view and ROI selection from virus infected barrel cortex L2/3; (right side) representative whole frame and individual traces from 1 whisker stimulation trial. **(B-B'')** Average Ca^{2+} transient amplitude, duration and number of events in spontaneous trials in density plots and bar graphs (insets). **(C-C')** Onset and decay times of Ca^{2+} transients in WT and *Gabra1* KO mice. The average was taken from all imaging sessions for individual neurons (N=459 neurons from 5 *Gabra1* KO mice, N=418 neurons from 4 WT mice). Statistics: linear mixed-effects models and Tukey post hoc tests. All bar graphs are represented as mean ± SEM. *p≤0.05, **p≤0.01, ***p≤0.001.

Suppl. Figure 2. Spontaneous L2/3 pyramidal neuron activity in Gabra2 KO mice. (A) Field of view and ROI selection from virus infected barrel cortex L2/3; (right side) representative whole frame and individual traces from 1 whisker stimulation trial. **(B-B'')** Average Ca^{2+} transient amplitude, duration and number of events in spontaneous trials in density plots and bar graphs (insets). **(C-C')** Onset and decay times of Ca^{2+} transients in WT and *Gabra2* KO mice. The average was taken from all imaging sessions for individual neurons (N=370 neurons from 4 *Gabra2* KO mice, N=307 neurons from 3 WT mice). Statistics: linear mixed-effects models and Tukey post hoc tests. All bar graphs are represented as mean ± SEM. *p≤0.05, **p≤0.01, ***p≤0.001.

Suppl. Figure 3. Changes in α1, α2, α3 $GABA_AR$ subunit expression in *Gabra1* and *Gabra2* KO mice. (A) Whole cell protein lysates were prepared from barrel cortices of WT &

Gabra1 KO littermates and WT and *Gabra2* KO littermates (5 mice per group) and Western blot (WB) analysis was performed for gephyrin, α2, α3 and normalised to total actin level. **(A')** Quantification for gephyrin, α2, α3 protein expression changes between WT and *Gabra1* KO. **(B)** WB analysis for gephyrin, α1, α3 and normalised to total actin. **(B')** Quantification for gephyrin, α1, α3 protein expression changes between WT and *Gabra2* KO. Statistics: Student's t-test (unpaired). All bar graphs are represented as mean ± SD. *$p \leq 0.05$, **$p \leq 0.01$, ***$p \leq 0.001$.

Suppl. Figure 4. L2/3 pyramidal neuron activity in *Gabra1*$^{flox/flox}$ and *Gabra2*$^{flox/flox}$ mice. **(A)** An overview of the viral infection *in vivo* in *Gabra1*$^{flox/flox}$. The Area 1 received AAV6-CaMKIIα-RCaMP1.07, while Area 2 received a combination of the AAV6-CaMKIIα-RCaMP1.07 and AAV8-CaMKIIα-eGFP-Cre as illustrated. **(B)** Example image of area2. White arrow heads: examples of neurons positive for RCaMP and Cre. **(C-D)** Field of view and ROI selection from Area 2 from *Gabra1*$^{flox/flox}$ or *Gabra2*$^{flox/flox}$. Upper panel: RCaMP and CaMKIIα-eGFP-Cre expressing neurons. Lower panel: RCaMP only expressing neurons. Right side: representative whole frame and example traces from RCaMP- and CaMKIIα-eGFP-Cre expressing neurons or RCaMP-only expressing neurons after whisker stimulation trial (shown as grey bar). **(E)** Comparing stimulation-induced amplitude change from Area 1 RCaMP expressing neurons with Area 2 RCaMP expressing neurons as density plot and bar graph (inset). **(F-F'')** Spontaneous Ca^{2+} transient amplitude, duration and number of events shown as density plots and bar graphs (inset) in RCaMP expressing neurons and RCaMP CaMKIIα-eGFP-Cre expressin neurons from *Gabra1*$^{flox/flox}$ mice. N=34 RCaMP neurons and N=47 RCaMP+Cre neurons from Area2 of *Gabra1*$^{flox/flox}$ mice. **(G-G'')** Spontaneous Ca^{2+} transient amplitude, duration and number of events in density plots and bar graphs (insets) comparing RCaMP-expressing neurons and RCaMP and CaMKIIα-eGFP-Cre-expressing

neurons from *Gabra2*$^{flox/flox}$ mice. N=58 RCaMP-expressing neurons and N=132 RCaMP+Cre neurons from *Gabra2*$^{flox/flox}$ mice. Statistics: linear mixed-effects models and Tukey post hoc tests. All bar graphs are represented as mean ± SEM. *p≤0.05, **p≤0.01, ***p≤0.001.

Suppl. Figure 5. Quantification of L2/3 cells infected with different AAV virus. (A) Example images of barrel cortex L2/3 cells infected with AAV6-CaMKIIα-RCaMP1.07, AAV6-CaMKIIα-CreERT2 and AAV6-hSyn1-flex-gephyrin mutants. The neurons were stained for CaMKIIα and GFP. Scale bar: 20 μm. (B) Quantification of average expression of RCaMP-expressing neurons (72 %) and neurons co-expressing RCaMP and eGFP-gephyrin mutants (40 %) after normalization to total CaMKIIα positive neurons.

Suppl. Figure 6. Spontaneous activity changes in L2/3 pyramidal neurons expressing mutant gephyrin. (A-A'') Average percentage changes after gephyrin-mutant expression for individual neurons are shown in bar graphs and the ratio are shown in violin plots to demonstrate the distributions for spontaneous Ca^{2+} transients. **(B)** Proportions of high- and lower-responding neurons before and after gephyrin-mutant expression *in vivo* selected based on Ca^{2+} transient amplitude. **(C)** Proportions of high- and lower-responding neurons before and after gephyrin-mutant expression selected based on number of events. eGFP, n=491 neurons; gephyrin-K148R, n=308 neurons; gephyrin-SSA, n=249 neurons; gephyrin-DN, n=204 neurons. Statistics: linear mixed-effects models and Tukey post hoc tests. All bar graphs are represented as mean ± SEM. *p≤0.05, **p≤0.01, ***p≤0.001.

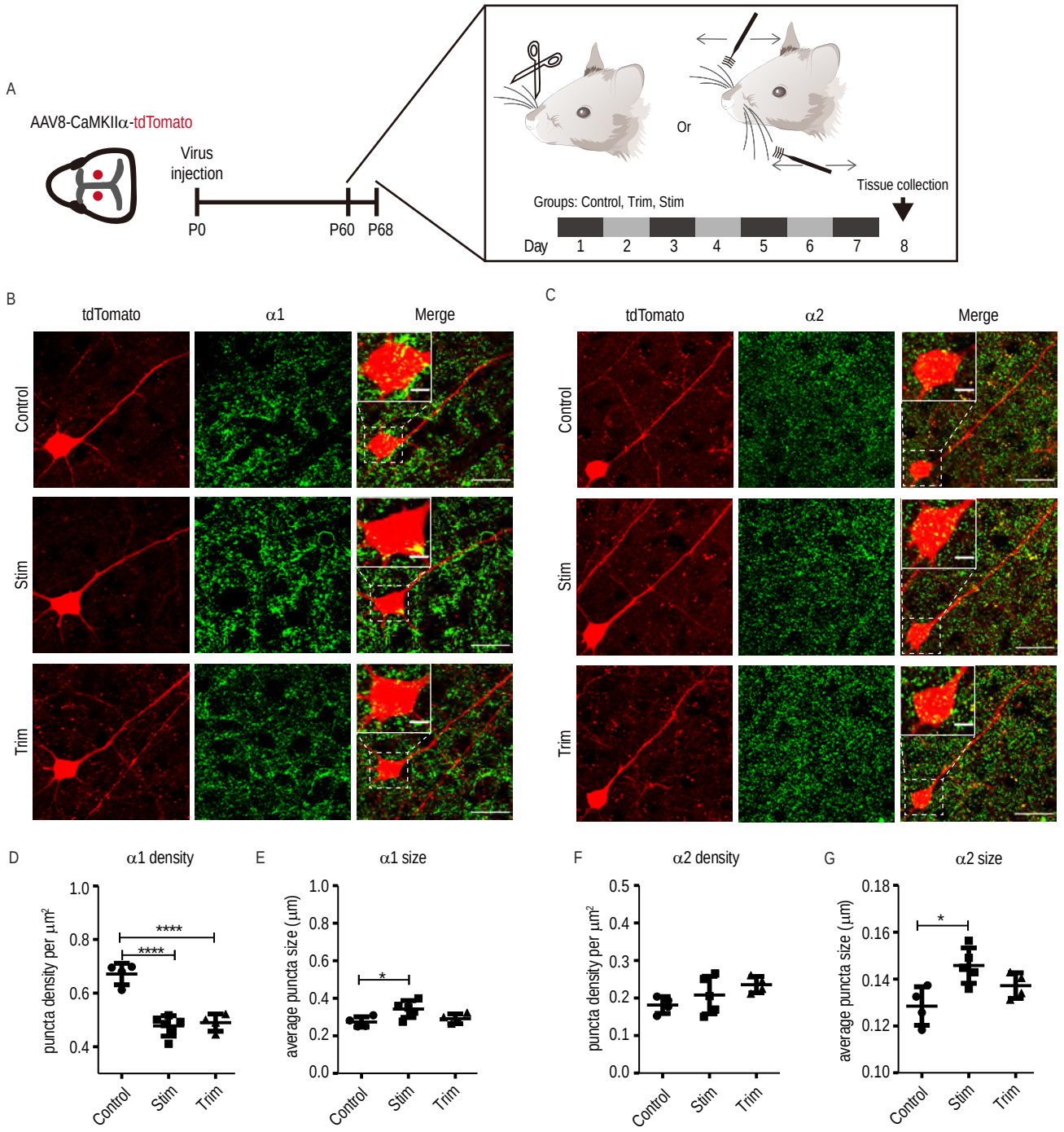
A
AAV8-CaMKIIα-tdTomato
Virus injection
P0
P60
P68
Or
Tissue collection
Groups: Control, Trim, Stim
Day 1 2 3 4 5 6 7 8
B
tdTomato
α1
Merge
Control
Stim
Trim
C
tdTomato
α2
Merge
Control
Stim
Trim
D
α1 density
puncta density per μm²
****
****
Control
Stim
Trim
E
α1 size
average puncta size (μm)
*
Control
Stim
Trim
F
α2 density
puncta density per μm²
Control
Stim
Trim
G
α2 size
average puncta size (μm)
*
Control
Stim
Trim

Figure 1.

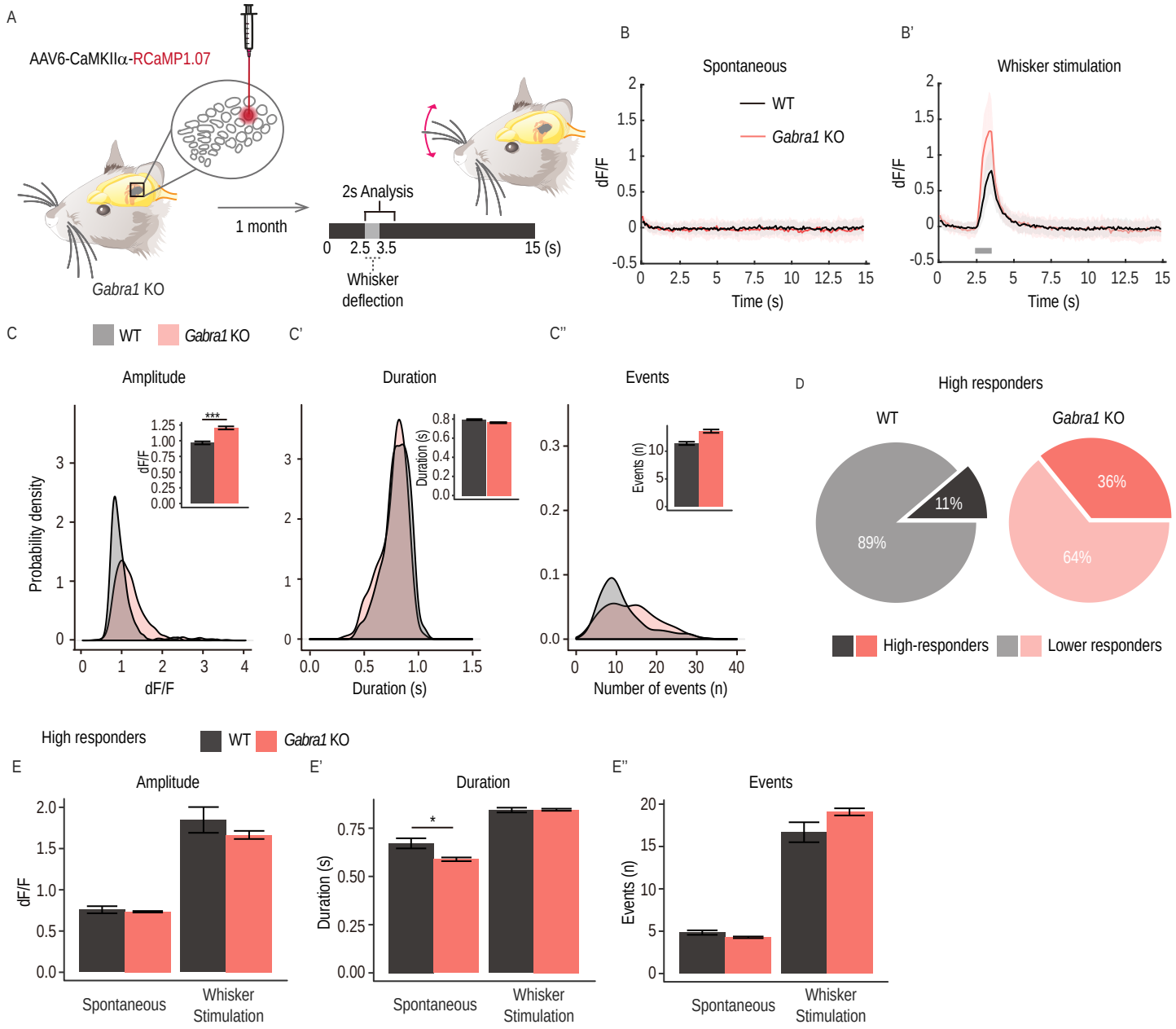
A
AAV6-CaMKIIα-RCaMP1.07
Gabra1 KO
1 month
2s Analysis
0 2.5 3.5 15 (s)
Whisker deflection
B
Spontaneous
WT
Gabra1 KO
dF/F
Time (s)
B'
Whisker stimulation
C
WT Gabra1 KO
Amplitude
Probability density
dF/F
C'
Duration
Duration (s)
C''
Events
Number of events (n)
D
High responders
WT
Gabra1 KO
11%
89%
36%
64%
High-responders
Lower responders
High responders
WT Gabra1 KO
E
Amplitude
dF/F
Spontaneous
Whisker Stimulation
E'
Duration
Duration (s)
E''
Events
Events (n)

Figure 2.

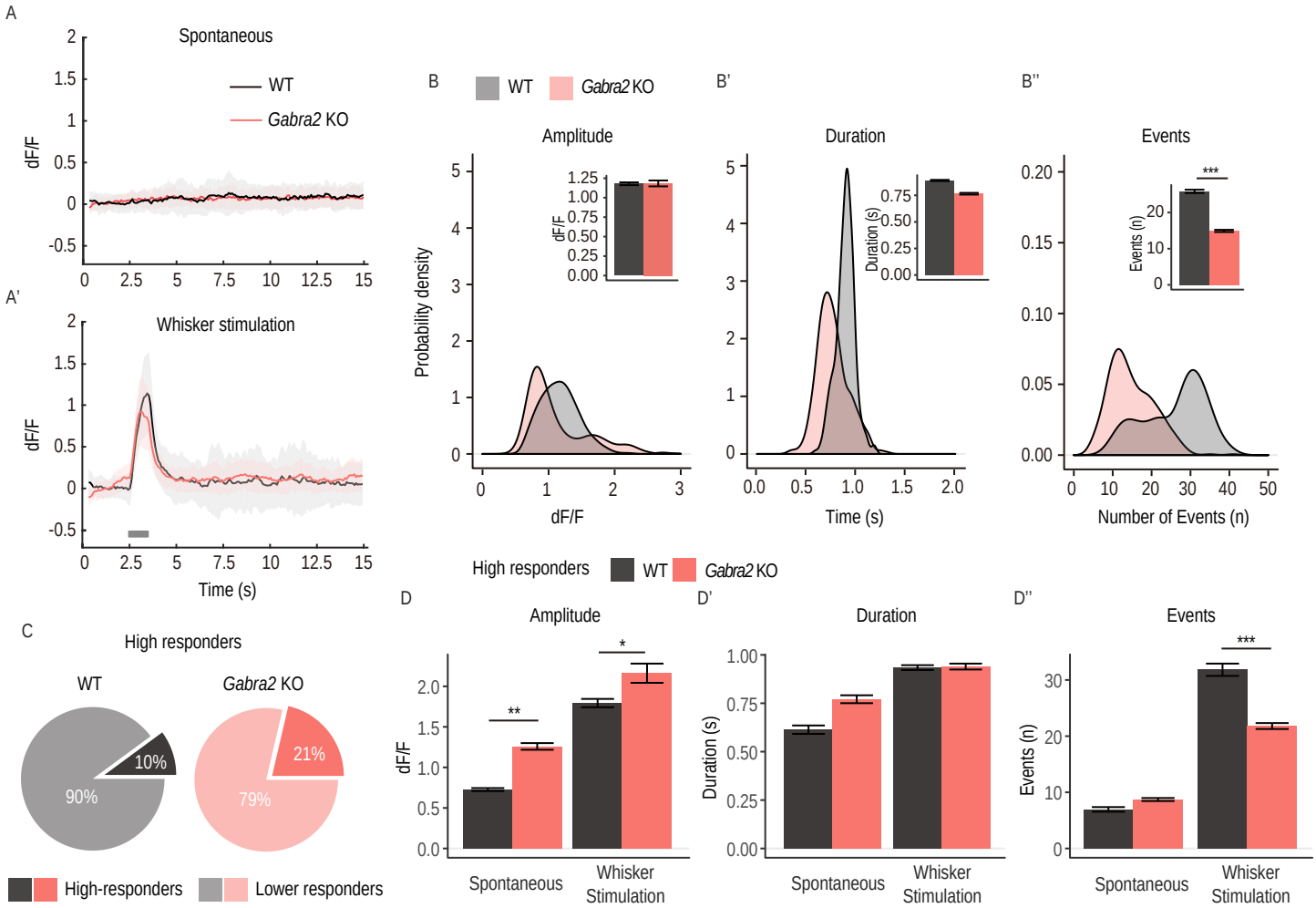
A
Spontaneous
WT
Gabra2 KO
dF/F
A'
Whisker stimulation
Time (s)
B
WT
Gabra2 KO
Amplitude
Probability density
dF/F
B'
Duration
Time (s)
B''
Events
Number of Events (n)
C
High responders
WT
Gabra2 KO
10%
90%
21%
79%
High-responders
Lower responders
High responders
WT
Gabra2 KO
D
Amplitude
Spontaneous
Whisker Stimulation
D'
Duration
D''
Events

Figure 3.

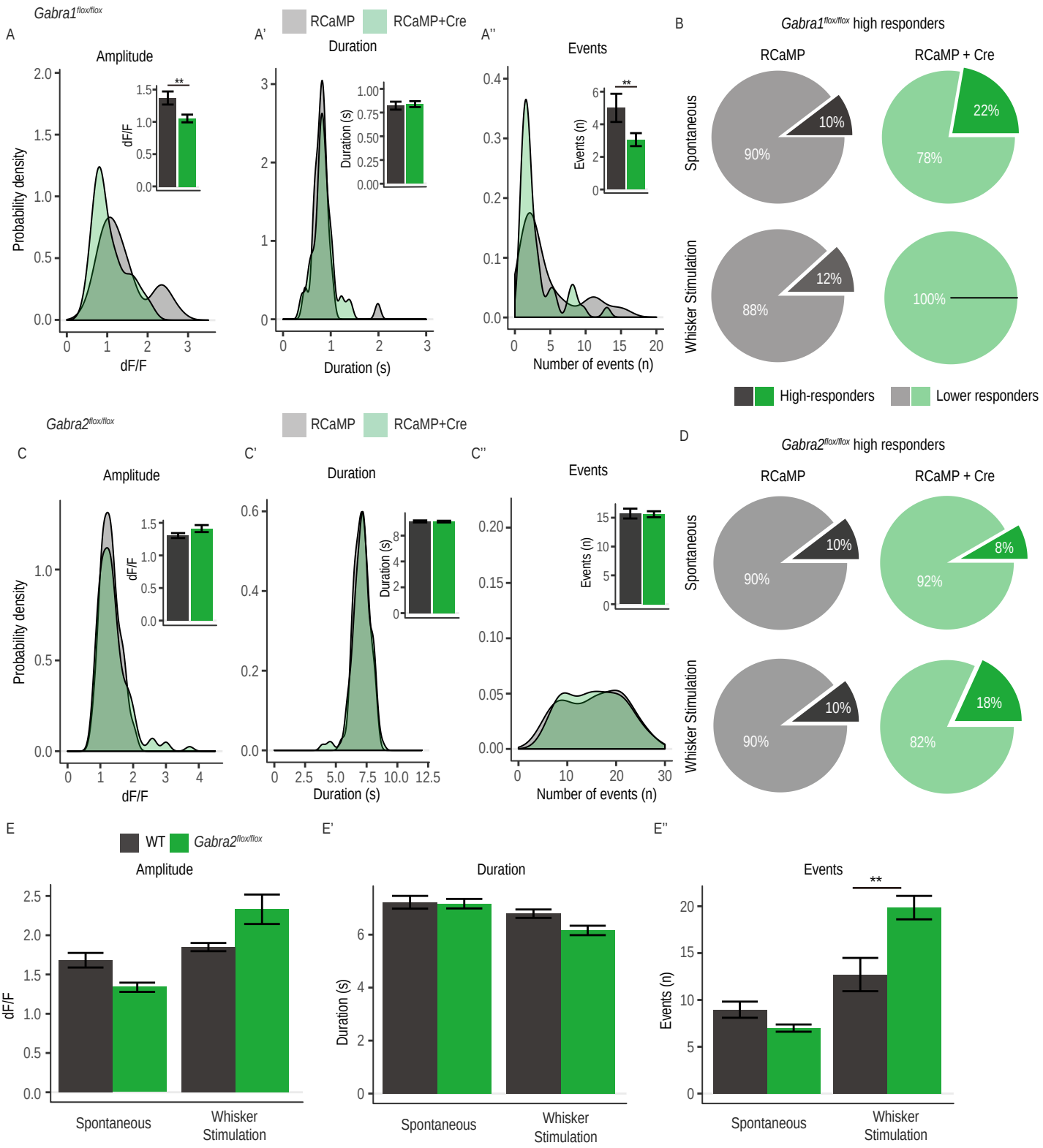
Gabra1flox/flox
A
Amplitude
Probability density
dF/F
A'
RCaMP
RCaMP+Cre
Duration
Duration (s)
A''
Events
Events (n)
Number of events (n)
B
Gabra1flox/flox high responders
RCaMP
RCaMP + Cre
Spontaneous
Whisker Stimulation
10%
90%
22%
78%
12%
88%
100%
High-responders
Lower responders
Gabra2flox/flox
C
C'
C''
D
Gabra2flox/flox high responders
10%
90%
8%
92%
10%
90%
18%
82%
E
WT
Gabra2flox/flox
E'
E''
Spontaneous
Whisker Stimulation

Figure 4

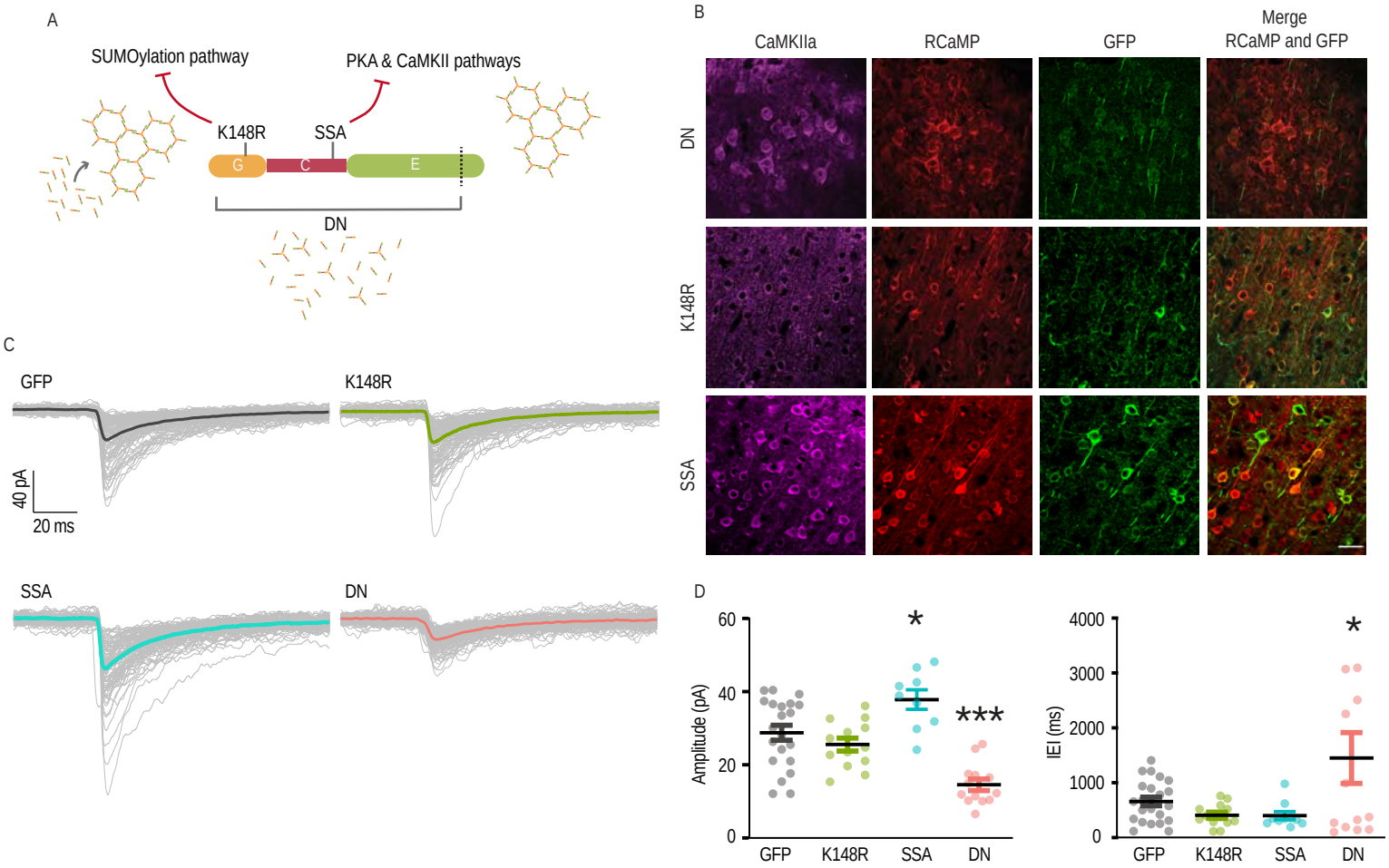
A
SUMOylation pathway
PKA & CaMKII pathways
K148R
SSA
G
C
E
DN
B
CaMKIIa
RCaMP
GFP
Merge
RCaMP and GFP
DN
K148R
SSA
C
GFP
K148R
40 pA
20 ms
SSA
DN
D
Amplitude (pA)
60
40
20
0
*
***
GFP
K148R
SSA
DN
IEI (ms)
4000
3000
2000
1000
0
*
GFP
K148R
SSA
DN

Figure 5.

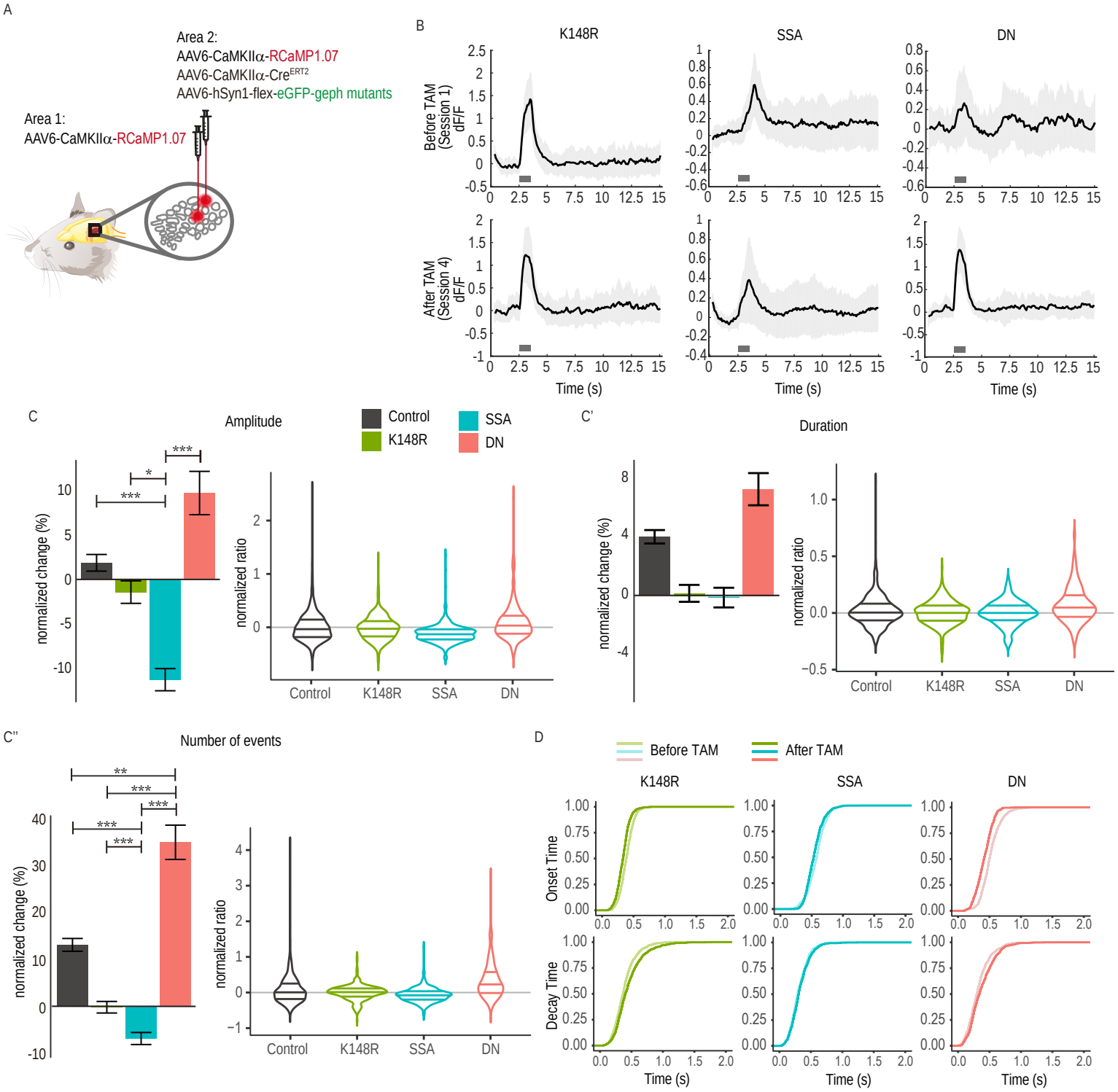
A
Area 2:
AAV6-CaMKIIα-RCaMP1.07
AAV6-CaMKIIα-CreERT2
AAV6-hSyn1-flex-eGFP-geph mutants
Area 1:
AAV6-CaMKIIα-RCaMP1.07
B
K148R
SSA
DN
Before TAM (Session 1) dF/F
After TAM (Session 4) dF/F
Time (s)
C
Amplitude
Control
K148R
SSA
DN
normalized change (%)
normalized ratio
C'
Duration
C''
Number of events
D
Before TAM
After TAM
Onset Time
Decay Time

Figure 6.